Laser Deposition of High Manganese Iron Alloy for Wear and Corrosion Resistance

by

Sujeet Shyamsunder Shinde

A thesis submitted in partial fulfillment
of the requirements for the degree of
Master of Science in Engineering
(Mechanical Engineering)
in the University of Michigan-Dearborn
2018

Master's Thesis Committee:

Professor Pravansu Mohanty, Chair
Assistant Professor Tanjore V. Jayaraman
Associate Professor German Reyes-Villanueva

ACKNOWLEDGEMENTS

First, I would like to thank my parents Shyamsunder Shinde and Lalita Shinde for supporting me throughout my entire education. Without their support this would not have been possible. I have been very fortunate to have Prof. Pravansu Mohanty as my advisor. I would like to thank Prof. Pravansu Mohanty for offering me a great opportunity to work on Direct Metal Deposition process in the Additive Manufacturing Process Laboratory at University of Michigan – Dearborn. I am grateful for his invaluable guidance and funding to make this work possible. He has taught me to be an independent thinker and has given me the freedom to explore, diversify and develop my own individuality during the course of this work. I am also thankful for the excellent example he has set for me as a professor and successful entrepreneur

I would also like to extend my thanks to Ramacharan Palacode Visveswaran, Vikram, Aniket Chandrashekar Jadhav, Neeraj Karmarkar, Vincent, Sharan, and Anup Bapat who have been working with me in the Laboratory, for their continuous guidance and support.

TABLE OF CONTENTS

LIST OF FIGURES

LIST OF TABLES

ABSTRACT

The usage of aluminum alloys for automotive applications has been growing rapidly. Research is being done to incorporate aluminum alloys as a replacement material for automotive components wherever possible. As aluminum itself has poor tribological properties, coatings are being developed to improve these properties. However, these conventional industrial coatings are not suitable to improve properties as they lack compatible materials and feasible manufacturing process. The purpose of this thesis is to develop low cost material with suitable manufacturing process that will improve the wear and corrosion properties of aluminum.

The material was iteratively developed from iron manganese (Fe-Mn) alloys which are used extensively in mining applications. Influence of aluminum, chromium and carbon additions were studied in order to improve both corrosion and wear resistance of the alloy. A laser cladding process was utilized to create desired alloys. To study the microstructure and other material properties, the deposited alloys was analyzed and tested for corrosion, wear, hardness, and x-ray diffraction. Wear resistance, corrosion, and hardness of the alloy was found to be superior to that of conventional cast iron and stainless steel.

Chapter 1 Introduction

1.1 Additive Manufacturing (AM)

Additive Manufacturing (AM) is defined as "the process of joining materials to make objects from 3D model data, usually layer upon layer, as opposed to subtractive manufacturing methodologies, such as traditional machining"[1]. It is also known as additive fabrication, direct digital manufacturing, layer manufacturing and solid freeform fabrication. With over two decades of history during its early stages AM was mostly used for the creating functional prototypes, also known as Rapid Prototyping (RP). The prototypes were then used as communication and inspection tools, resulting in prototypes manufactured in short time directly from solid CAD models reducing the time required for production stages[2]. Through intensive research over the last 20 years, significant progress has been made in the development and commercialization of AM processes, with applications in several industries such as aerospace, automotive, biomedical, and other fields. The most aggressive application being in aerospace and automotive. Some of the commonly known AM processes are Stereolithography, Fused Deposition Modeling [3], Selective Laser Sintering [4], Laminated Objective Manufacturing [5], 3-D Printing[6], and Laser Metal Deposition [7]. Additive manufacturing allows manufacturing of geometrically complex parts without need for fixtures as required in subtractive processes. AM processes are cost-effective for small batches of parts, significantly shorten the manufacturing time, and can build parts that are difficult to manufacture with subtractive manufacturing processes[8]. In this study we will be using the laser metal deposition (LMD) technique to develop new alloy.

With Laser Metal Deposition (LMD) also called as Direct Metal Deposition (DMD) technology, materials that are difficult to be cast and thermo-mechanically process, or that cannot be solidified successfully by powder metallurgy, can be easily manufactured. Features such as internal protrusions, which cannot be machined directly or require extensive machining, can be

formed. Materials that require multiple steps can be formed in a single step, eliminating the need for special fixtures, additional equipment, and space required with each additional step[9].

1.2 Direct Metal Deposition (DMD)

Laser assisted direct metal deposition refers to the additive manufacturing technique for building parts from a computer-aided design (CAD) model. Metal powders are directed into the laser focal zone and are melted with laser beam and then re-solidified into fully dense metal in the moving molten pool created by the beam. To control the motion of a laser focal spot over a part, a motion control program is developed according to CAD model. The Figure (1.1) below represents the basic working principle of direct metal deposition process[10].

Successive layers are then produced to develop the entire component representing the

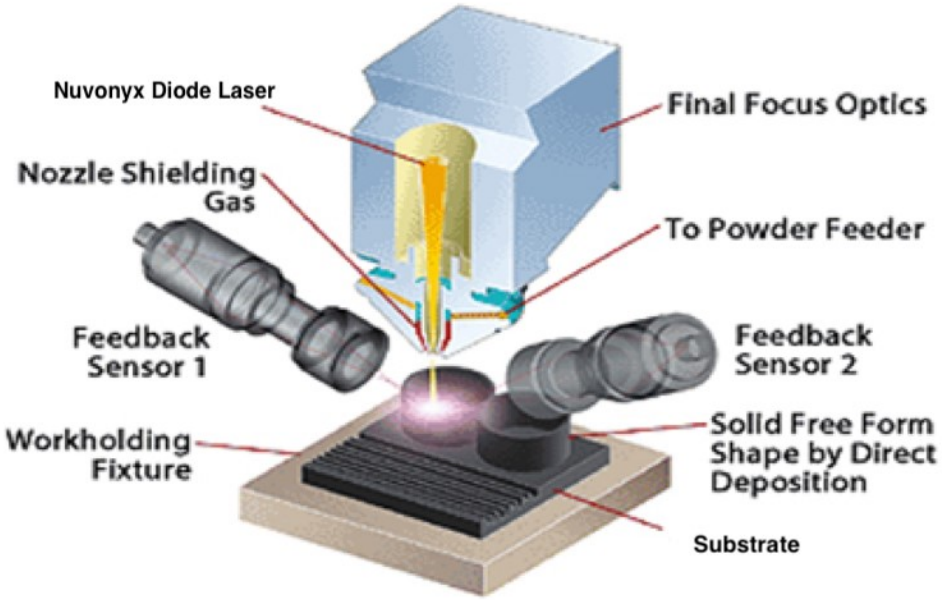

Figure 1.1 Direct Metal Deposition Process

desired CAD model. Motion paths are developed using CNC tool-path format (DLF) command motion for five motion axes. Additional axes control can allow additional degrees of freedom if required. Processing during the deposition of parts is performed usually in inert gas (nitrogen) environments, to reduce oxidation. Multiple powder compositions can be simultaneously fed into

the melt pool to produce alloying at the focal zone or provide material choice relative to certain location within a desired part[10].

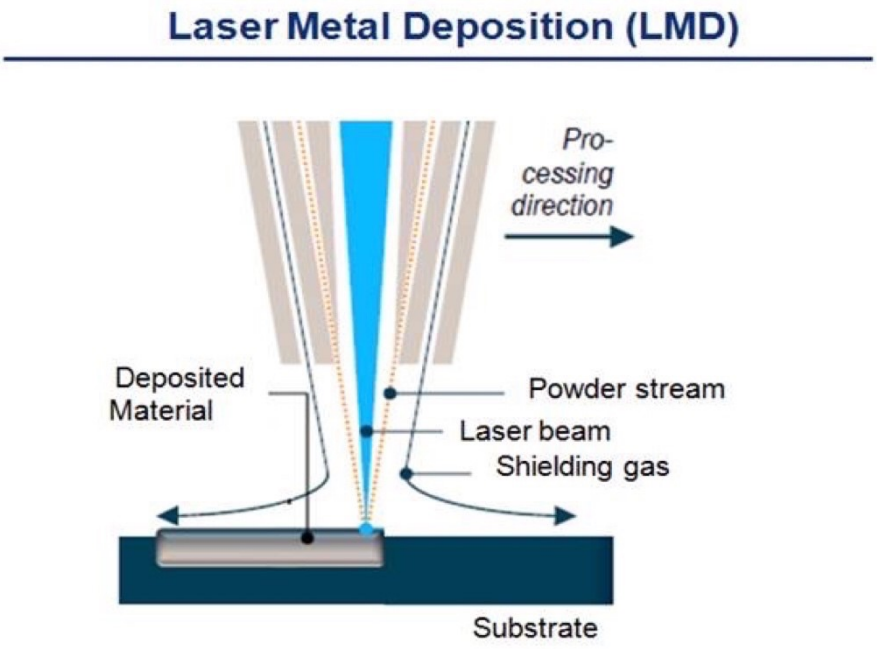

Figure 1.2 Laser Metal Deposition

Figure (1.2) shows the motion path of the laser deposition process. Each layer starts and stops at the part boundary until an entire first cross-sectional planar layer is formed by deposition of overlapping layers. The laser beam then moves away from the part depending upon layer thickness set by the motion system. The motion path which can be developed using CNC program controls the laser beam, powder feed and motion system to deposit linear layers of material that are laid side by side with fixed laps. Laser power, powder feed rate, and lateral velocity of beam are controlled to produce a full density layer of a given composition. Successive layers are deposited, and the entire part or features of a part assembly are then built additively[11].

Powders of desired compositions which can be pre-alloyed or pre-blended are directly fed into the molten pool through powder feeder. The ability to deposit unique alloys, and graded compositions, which can be pre-blended or combined at the focal zone, provide the capability to control properties within a manufactured part. The capability of DMD system to feed multiple alloy powders from multiple powder feeder system at the same time and ability to control their feed rates individually increases the flexibility and functionality of system. Any alloy composition

can easily be tried, by mixing the powders with appropriate particle size. Functional grades of the powder composition are developed by varying the feed rates up or down respectively with multiple feeders to obtain the desired powder composition gradients. Segregation in mixed powders, during agitation by feed systems can be eliminated, by feeding powders of different size separately[10][9].

1.3 High Manganese Iron Alloy

The focus of this study is to develop a high manganese iron alloy as a coating material to enhance the wear and corrosion resistance of aluminum components. Compared to conventional stainless-steel High manganese iron alloys have exceptional hardness and wear resistance. Fe-Mn or the Iron-manganese alloy was discovered in 1888 by Sir Robert Hadfield. The alloy has gained considerable interest particularly in automotive industry because of its high strength and ductility properties. The presence of manganese in the Fe-Mn system is known to induce transformation or twinning of austenite phase resulting in unique work hardened material. Fe-Mn binary system which are used in automotive industry as TWIP (TWinning Induced Plasticity) and TRIP

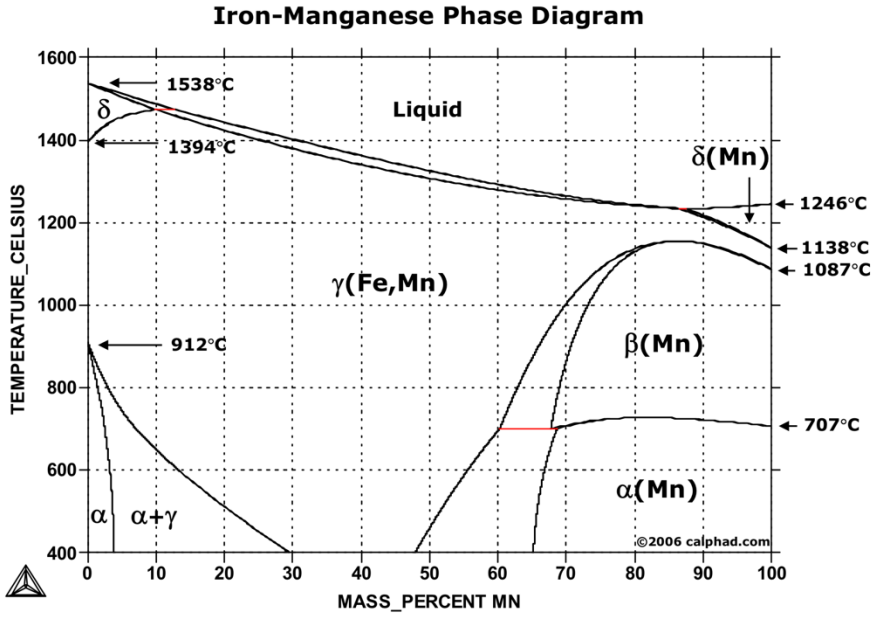

Figure 1.3 Iron-Manganese Phase Diagram

(TRansformation Induced Plasticity) represent a potential low-cost wear material compared to other alloys. The presence of manganese in these alloys reduces corrosion resistance but the

corrosion properties can be improved by addition of chromium and aluminum as alloying elements[9].

Fe-Mn Phase diagram as shown in Figure (1.3). The different phases that can be expected at different temperature and manganese content can be interpreted from the phase diagram. At the pressure of 101325 Pa the melting point of iron and manganese is 1538 °C and 1246 °C, respectively.

Direct metal deposition technique is used as a manufacturing technique to melt the predetermined mixture of Fe-Mn alloy in this study. Direct metal deposition process has a advantage that the solidification rates achieved in the process are similar to that of the gas atomization of powders which are commonly used to manufacture precursors for coating deposition processes. To begin with, steel substrates were used to make this alloy[9].

1.3.1 Stainless Steel 316

Stainless steel 316 was used as substrate for the sample deposition. The substrates used were from McMaster-Carr Supply Company. The following Figure (1.4) shows the composition of SS 316 substrate.

Material Composition	
Iron	58.23-73.61%
Carbon	0-0.08%
Chromium	16-18.5%
Copper	0-1%
Manganese	0-2%
Molybdenum	0-3%
Nickel	10-15%
Nitrogen	0-0.1%
Phosphorus	0-0.045%
Silicon	0-1%
Sulfur	0.35%
Titanium	.7% Max.

Figure 1.4 Stainless Steel 316 composition in wt.%

1.3.2 Stainless Steel 304

Stainless steel 304 was also used for the deposition of samples. SS-304 used was also from McMaster-Carr Supply Company. The following Figure (1.5) shows the composition of SS 304 substrate.

Material Composition	
Iron	53.48-74.5%
Carbon	0-0.08%
Chromium	17.5-24%
Cobalt	0-0.29%
Copper	0-1%
Manganese	0-2%
Molybdenum	0-2.5%
Nickel	8-15%
Nitrogen	0-0.1%
Phosphorus	0-0.2%
Silicon	0-1%
Sulfur	0-0.35%

Figure 1.5 Stainless Steel 304 composition in wt.%

1.3.3 Low Carbon Steel

Low carbon steel was also used for the deposition of samples to see if there is change in deposition quality. LCS used was also from McMaster-Carr Supply Company. The following Figure (1.6) shows the composition of LCS substrate.

Material Composition	
Iron	98.06-99.42%
Carbon	0.13-0.20%
Manganese	0.30-0.90%
Phosphorus	0.04% Max.
Silicon	0.15-0.30%
Sulfur	0.50% Max.

Figure 1.6 Low Carbon Steel composition in wt.%

Chapter 2 System Descriptions and Analysis

2.1 DMD 105D System Description

Figure 2.1 DMD 105D 3D Printer

A 5-axis Direct Metal Deposition System as shown in Figure (2.1) (Part No. DMD 105D, University of Michigan,) manufactured by POM Group, Inc. is equipped here at Additive Manufacturing Process Lab (AMPL) in University of Michigan-Dearborn. Coordinate values for each axis are taken up to three digits after decimal point. Using computer numerical control (CNC),

the five defined axes are able to travel within the range of: 350mm for X, 300mm for Y, and 350mm for Z, ±45˚ for B (rotatory motion along Y axis) and 360˚ for C (rotatory motion along Z axis). The system itself has a 3D static accuracy of ±75 microns and a repeatability of ±9 microns over workspace[12].

The DMD system is generally made up of four sub systems: laser system, powder feeder system, gas system and controller. There are two laser systems used here. The DMD system was equipped with a 1 Kw Nuvonyx Diode Laser (Nuvonyx, Inc.) of a wavelength of 805±10 nm. The spot size of laser beam for the system is about 2000 microns in diameter at the stand-off height of nozzle (13.5mm from nozzle tip to melting zone). A second backup laser (Disk laser) is also equipped into the system. It's also a 1Kw Trumpf disk laser (Part No. TruDisk 1000, University of Michigan, Government Funded No381798). The Trumpf laser has a wavelength of 1030 nm. At the standard stand-off height, a 50-micron laser beam diameter is observed. The Laser beam first travels through fiber optic cable and then enters a collimator. The laser beam can be narrowed in collimator to make it more aligned in any one direction. Two 45˚ oriented mirrors are used to reflect the laser beam. Before entering the nozzle the laser beam travels through focusing lens and is collinear with nozzle axis [10] [12].

Four processing gases are used in the DMD system: argon, helium, nitrogen and air. Pressurized air is used for controlling pneumatic systems and it is also used for cooling of laser lens to avoid fogginess on lens. Nitrogen is used for powder hopper cover gas and carrier gas. The cover gas is used to keep stable pressure in deposition chamber while carrier gas is used for delivering of powder into melt pool. To focus the flow of powder directly into the melt pool from the exit of nozzle nitrogen also serves as shaping gas. During deposition process, the melt pool is shielded by pressurized nitrogen gas to keep the melt pool from oxide or nitride formation[12].

In this study the powders are stored in two powder feeders known as hoppers. A total of four hoppers are installed in the DMD system, but they are of different feed rate ranges. Recommended powder size for the system used is in between 45 to 150 microns [12]. Narrow and spherical powder shape help improve the powder flow in the system. To eliminate any moisture content in the powder the powder is first put into furnace and then used in the system [10] [12].

A computer aided manufacturing (CAM) software package was already installed with the DMD system which is called DMD CAM. After creating a 3D model using CAD software the 3D model would be loaded to DMD CAM package and then precise toolpaths and related CNC programs would be generated by the system. The movement of nozzle is programmed for each layer of deposition to move upward. This strategy protects the nozzle to avoid any collision and also gives sufficient cooling time for deposited part. For some simple structures, the forward and backward motion of nozzle is unnecessary and leads to wastage of time. To avoid this, a MATLAB program is used to generate the motion of nozzle and the coordinates are saved in a .txt file[12].

The CNC programming is similar to other standard systems only difference being the coordinate system. The command lines coded in the MATLAB are fixed and only point coordinate values are changed for desired tool path as per the CAD geometry. The CNC data points are recorded and a .TXT file is generated. The .txt file is then converted into .sub file which will be the input file extension for DMD system. This process is very convenient for simple geometry such as line or square. The MATLAB program which is used for generating CNC program for DMD is also readily available[12].

A Closed Loop Feedback User Interface is implemented in the DMD system to control the components of system. Three cameras distributed 120˚apart are used to view focused image of the melting. The image captured by these cameras are then transferred to the closed loop PC to process the images. The processing of images is done using real time CNC data and the position of laser beam and other system components is adjusted accordingly. The closed loop feedback control system is used to control build quality and build height. To improve the deposition quality and to eliminate the height variation, CNC programs play an important role. The starting points can be varied for each layer to avoid excess building at one spot. To avoid the problem with over building in any one spot the nozzle movement should be continuously varied clockwise and anti-clockwise for each subsequent layer [10] [12].

2.2 Hopper Test

The powder hopper test is carried out to know how much powder is delivered at the end of nozzle exit. The amount of powder delivered depends upon the hopper feed rate. The hopper feed rate depends upon the how fast the feeding wheel rotates. The hopper test is carried out under same cover gas and carrier gas flow values that will be used during the deposition.

The hopper test gives us an idea on how the powder is flowing through powder feeder to the nozzle exit. The flow of powder varies from powder to powder along with particle size distribution. It is necessary to know if the powder is flowing smoothly. A container is placed at the end of nozzle exit and the test is run for 1 minute. The amount of powder that is collected is then weighed and measured in grams/minute. The results of hopper test carried out for the powder that we used for deposition are given below in the Table (1).

Table 1 Hopper Test results

Feedrate	Gas Values (SLPM)		Powder Flow (g/min)
	Cover Gas	Carrier Gas	
1000	6	6	3.8
1200			4.7
1400			5.5
1600			6.2
1800			7.0
2000			7.8

2.3 Laser Power Test

Laser power test gives an insight to the Power produced by laser in Watts at different Current (Ampere) values. The power produced at certain Current (Ampere) value depends upon the condition of system. The power values also give important information for the maintenance of system. Since the values vary depending upon the system condition it is important to know these values as it affects the deposition process. The power generated at the laser is never the same the power values obtained at nozzle exit as certain amount of power is lost during the transmission. If the total laser power loss is within 10-12%, the system is treated to be in good working condition. If the loss exceeds 12% further maintenance needs to be performed on the system. The power losses can be reduced by using proper methods such as proper beam alignment, cleaning of lenses and mirrors, cleaning of nozzle exit from any deposition of particles[10].

The power test was carried out on Nuvonyx diode laser and the values were recorded using laser power meter (Pyrometer). The distance between Pyrometer surface and nozzle exit was kept between 20 to 25 mm. The input laser power was generated using two power supply. Both power supply was given same input values and were increased by 2 amperes for each new measurement. Following Table (2) shows the power and voltage values obtained at different current values.

Table 2 Laser Power Test

Current (Amperes)	Power (Watts)	Voltage (V)
10	25	48.7
12	57	49.1
14	95	49.4
16	135	49.7
18	172	50.0
20	210	50.3
22	248	50.6
24	285	50.8
26	325	51.0
28	358	51.2
30	390	51.4
32	418	51.6

34	448	51.8
36	470	52.0
38	495	52.2
40	516	52.4
42	542	52.8

2.4 Microstructure Analysis

2.4.1 Scanning Electronic Microscope (SEM) & Energy Dispersive Spectroscopy (EDS) Analysis

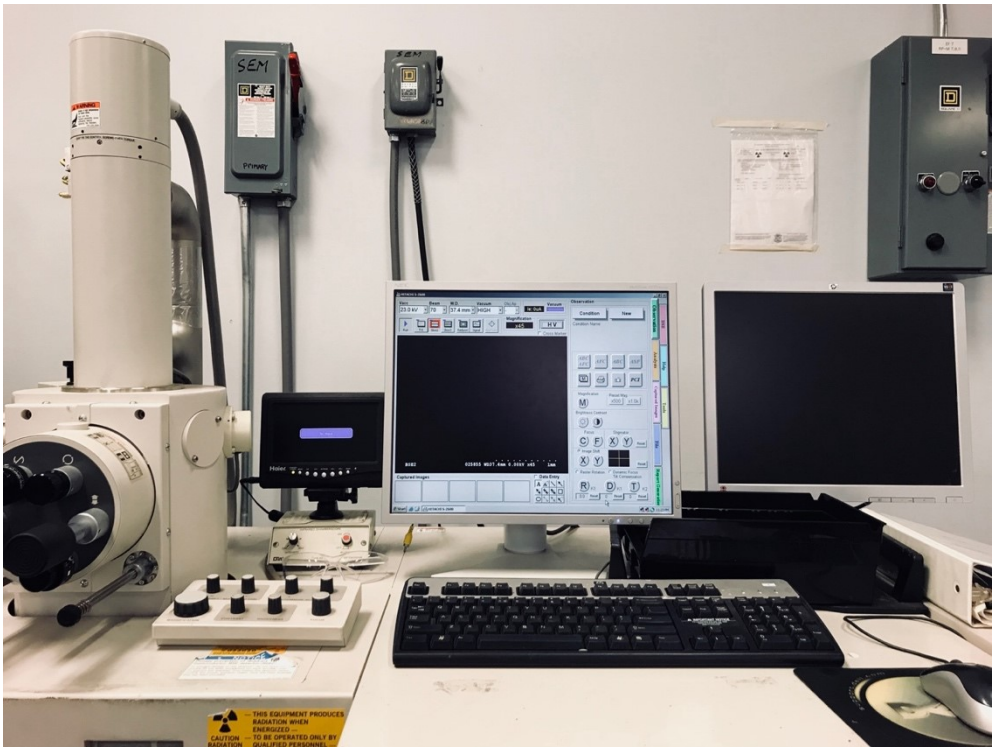

Figure 2.2 SEM and EDS analysis machine

The microstructure of sample deposits was analyzed using a Hitachi Scanning Electron Microscope (SEM) (Model S-2600N, University of Michigan Property 374500). As shown in figure (2.2).

The Figure (2.3) below represents the basic working principle of SEM and EDS. The SEM scans a sample surface with a finely converged electron beam in a vacuum, detects the information

(signals) produced from the sample, captures an enlarged image of the sample surface, and displays on the monitor screen.

Irradiation of an electron beam in a vacuum chamber and on to the sample surface generates multiple x-ray signals such as characteristic X-rays, secondary electrons (SE), backscattered electrons (BSE), and other signals are generated as indicated in the figure above. Images of sample

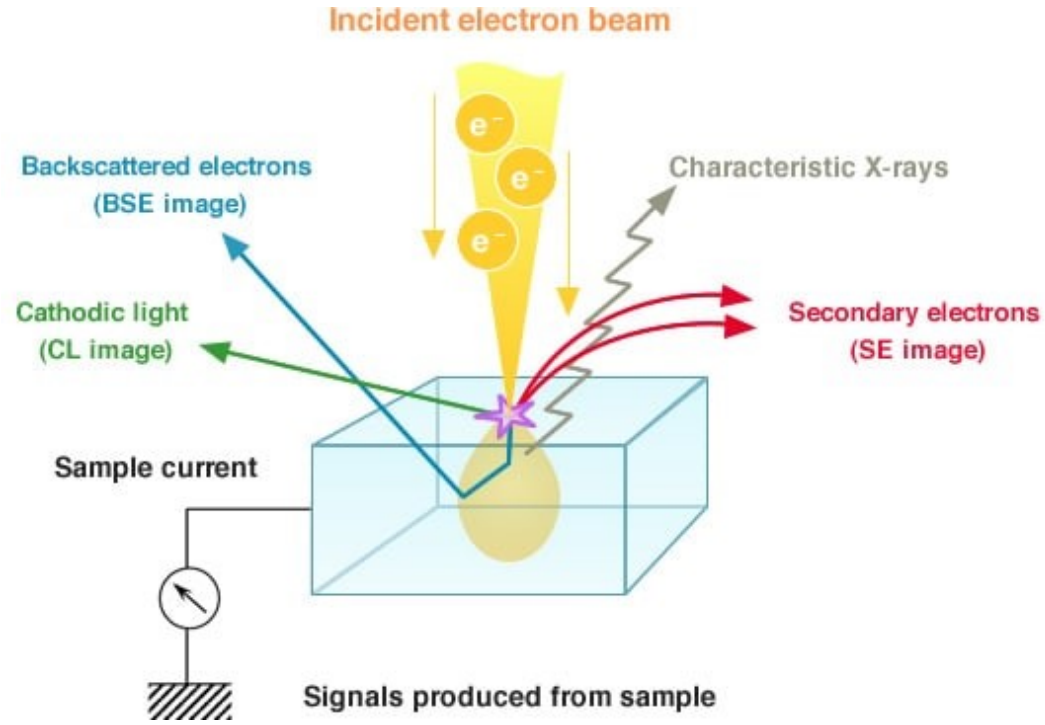

Figure 2.3 SEM working principle

surface are generated by using Secondary and Back-Scattered electrons. The topographical structure of the sample is obtained from detection of Secondary electrons (SE) produced near the surface of sample. To determine the composition of sample Backscattered electrons (BSE) are used as they reflect the sample and depends upon atomic number, crystal orientation of the sample. A BSE image, therefore, reflects the compositional distribution on the sample surface. An X-ray detector can be mounted to the SEM for conducting elemental analysis using Energy-Dispersive X-ray analysis. Hence the SEM serves two purposes. One for observing the sample structure, and second for determining the elements and their composition amount in the sample[13].

The deposition structure was studied layer by layer as the deposition was done. Height wise the SEM images of Surface layer, Middle layer, and the Interface layer were captured and studied.

The composition of deposition was studies using Energy-Dispersive Spectroscopy. The analysis was done at nine different points on the sample. Three points on the Surface layer, three points on the middle layer, and three points on the Interface layer. The composition of different metals was studied during the analysis. EDS mapping was also carried out on sample at random position to study how well each metal powder was distributed during the deposition.

2.4.2 Wear Test

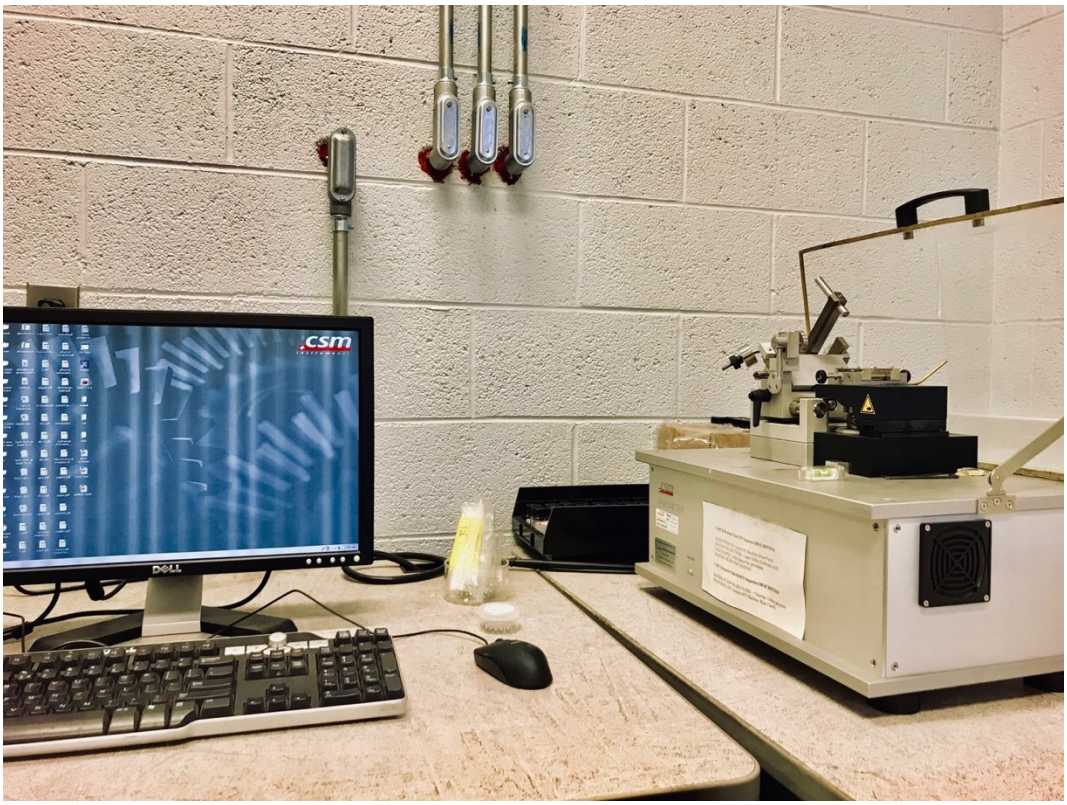

Figure 2.4 Wear Testing machine Tribometer CSM

The complete wear test was carried out in two parts. The first part was done using CSW Tribometer (model TRB) shown in Figure (2.4). The tribological behavior of the deposited alloy was studied using the CSW Tribometer. The tribometer probe is placed on the sample surface under a precise load of 5N which is constant for all the samples tested. The sample then reciprocates in a linear track horizontally on the samples for 8000 cycles. The ball used for wear test were tungsten carbide balls and the same was used for all the samples tested. All the samples were polished to mirror finish before performing the wear testing. When conducting tests, the samples mounted and the tribometer probe were both kept flat using spirit level.

2.4.3 Wear Depth Profile Test

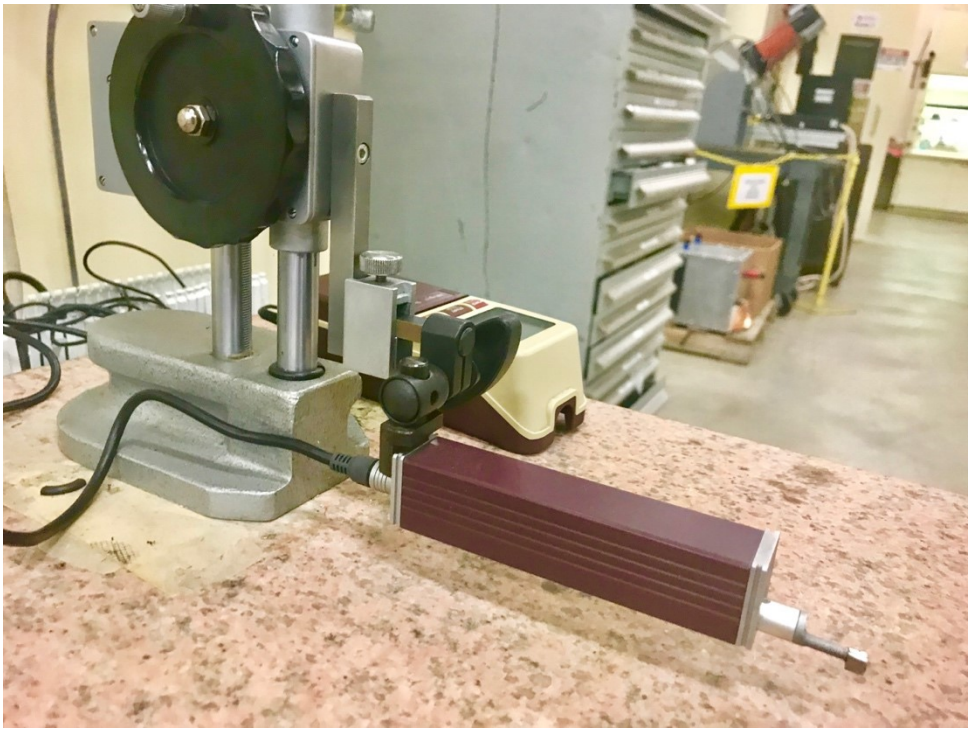

Figure 2.5 Wear Depth Profile testing machine

After the wear test were performed the samples were placed under a profilometer to measure the depth of wear profiles as shown in Figure (2.5). The probe of the profilometer is placed on the samples at the center of the wear profile which then moves for a length 6mm perpendicular to direction of the profile. The depth values were then recorded and plotted in excel as output. The stylus type Mitutoyo surface measurement tester was used for measuring the depth of the wear.

2.4.4 Hardness Test

Figure 2.6 Vickers Hardness testing machine

The hardness testing was carried out by using the Struers Microhardness Tester (University of Michigan Property 572831) shown in Figure (2.6). The hardness was measured using Vickers hardness scale for a load of 0.3 Kg. The load was applied for 10 seconds and the hardness values were calculated using the width of diamond shape indent on the sample. The width is then compared with Vickers scale to determine the hardness. Hardness was measured on 9 different places on each sample. Three readings on the surface, three readings on the center on deposition and three readings on the interface. All the hardness readings were taken on the same sample used for SEM & EDS analysis.

The Figure (2.7) represents the points where hardness readings were recorded. One advantage of recording readings at multiple points on sample is that it gives us information about uniformity in distribution of elements and its deposition.

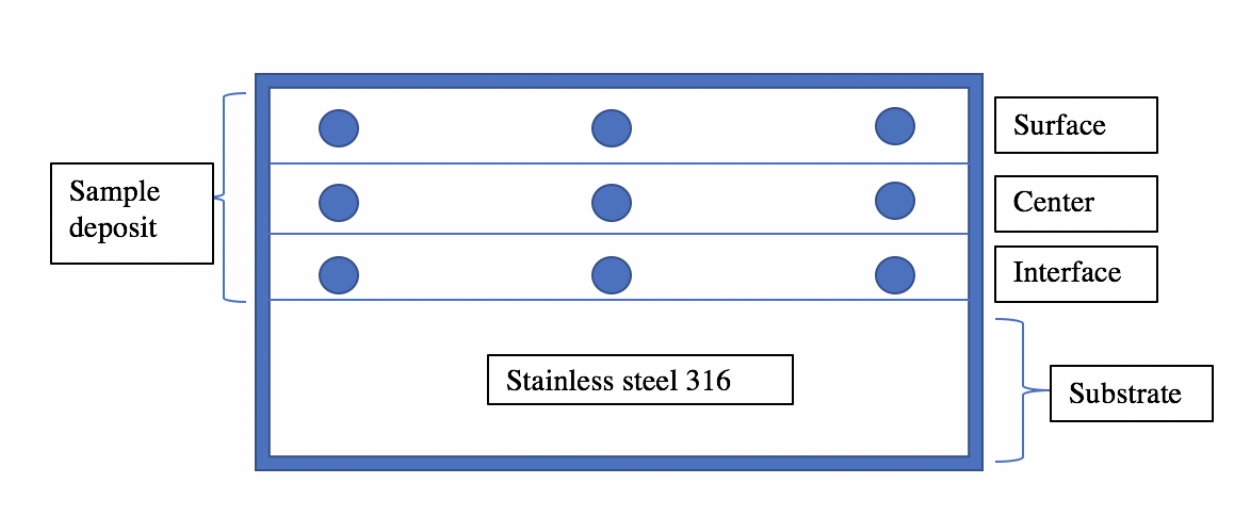

Figure 2.7 Location of hardness points on deposited samples

2.4.5 X-Ray Diffraction

X-Ray diffraction is a non-destructive tool for identification of crystalline phases of various materials. X-ray diffraction techniques are superior compared to other techniques in elucidating the three-dimensional atomic structure of crystalline solids. Figure (2.8) represents the basic working principle of XRD. The properties and functions of materials largely depend on the crystal

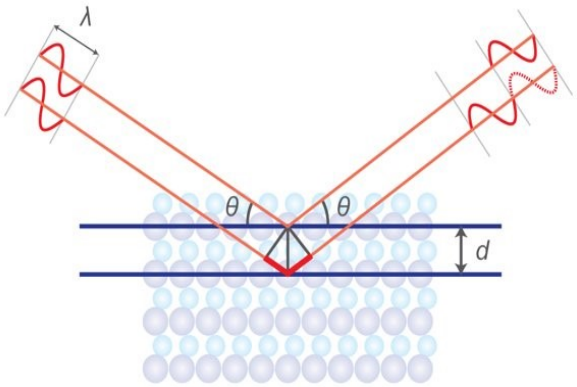

Figure 2.8 XRD working principle

structures.

The X-Ray diffraction works on the principle of Braggs equation:

$$n\lambda = 2d\sin\theta$$

where n is an integer, λ is the characteristic wavelength of the X-rays impinging on the crystallize sample, d is the interplanar spacing between rows of atoms, and θ is the angle of the X-ray beam with respect to these planes. When this equation is satisfied, X-rays scattered by the atoms in the plane of a periodic structure are in phase and diffraction occurs in the direction defined by the angle θ. This diffraction pattern can be thought of as a chemical fingerprint, and chemical identification can be performed by comparing this diffraction pattern to a database of known patterns[14].

Figure 2.9 Rigaku XRD testing machine

To perform the phase analysis and determine the crystal structure of the samples and the powders X-Ray Diffraction tests were carried out. The tests were executed using Rigaku Miniflex XRD (Cu Kα radiation with λ = 1.5402 0A) machine (Michigan Registration Num. 26423) as shown in Figure (2.9).

2.4.6 Corrosion Test

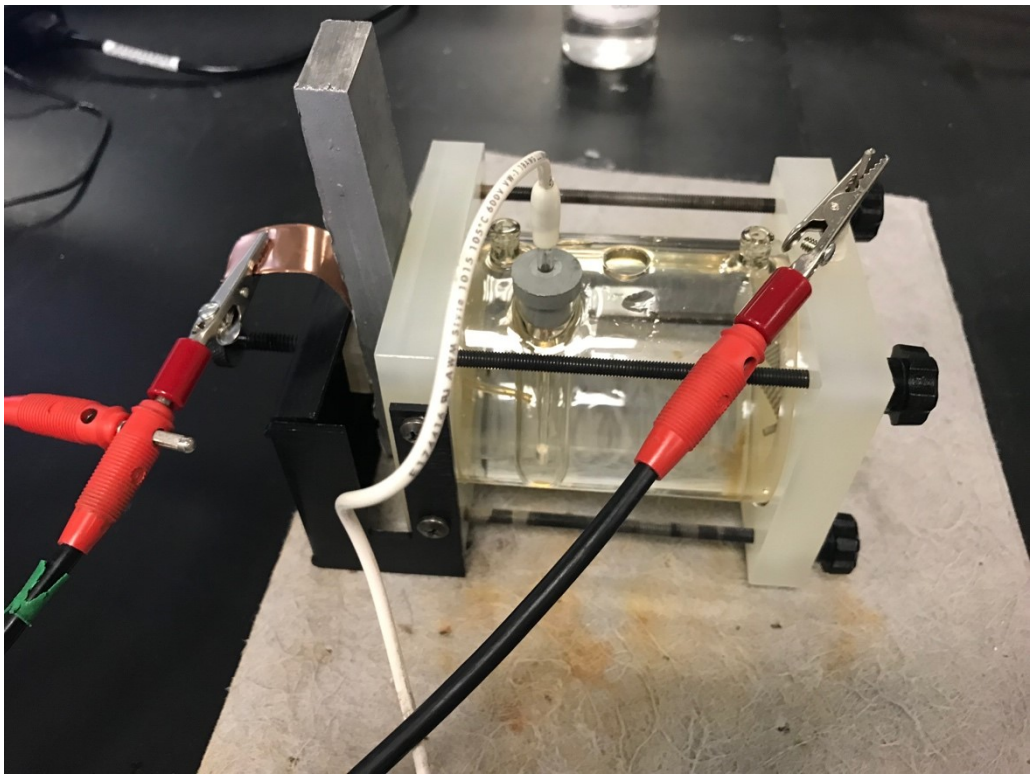

Figure 2.10 Corrosion testing setup

The corrosion testing of the samples was performed by using an AMETEK Princeton Applied Research (PAR) Flat Cell model K103. Figure (2.10) shows the corrosion testing setup. The surface of the corrosion specimens was grinded on 240-800-grit emery paper and were cleaned with distilled water and alcohol prior to each corrosion test. To establish the free corrosion potential (Ecorr) all samples were kept in solution before polarization. To evaluate the galvanic current Zero Resistance Ammetry (ZRA) technique was implemented. Anodic polarization tests were carried out in a 0.5-wt. % NaCl solution prepared using analytical grade reagents. The initial pH value of the solution was 5.8 and the initial temperature of the solution was at 22°C. The specimen was driven from an Ecorr value of −1 to 2V (vs ref) at a scanning rate of 1.66 mV/s to produce potentiodynamic polarization graphs. All potentials were measured with reference to a standard electrode, saturated calomel electrode (SCE). Apart from the alloy samples tests were also carried out on aluminum, stainless steel 316, and cast-iron samples[9].

Chapter 3 Alloy Development

Conventional alloying methods have certain limitations that are difficult to overcome. Alloys with phases that have higher melting points are difficult to melt, solidification of alloy is slow and resulting in segregation and separation of constituent's phases in the alloys. To overcome these issues alternate approaches can be used such as use of atomized powders, but the cost and time involved are huge in these processes. In direct metal deposition technique using laser as a source of heat with high power density provides a clean thermal energy. The clean heat source can provide homogeneous micro-structure and can adapt to change in variation[9].

High manganese steel alloys are known for their properties such as high tensile strength and high wear resistance. The mechanical properties of these high manganese steels can be varied by varying the manganese content in them. In this study a combination of Fe-Mn-Cr-Al-C are studied for wear and corrosion resistance[9].

3.1 Effects of Alloying Elements

Manganese is a strong austenite former and is also a potential cost-effective replacement for nickel. The disadvantage of manganese is the tendency form beta manganese by segregation and also its high affinity for oxygen at higher temperature. This often results in the alloy with depleted manganese content at higher processing temperature. Manganese stabilizes the austenite phase and prevents the formation of e martensite phases. Carbon and Nitrogen both have higher solubility in austenite matrix. Carbon is also a strong austenite former that also significantly increases mechanical strength, but excess content can lead to brittleness. Chromium increases the resistance to oxidation at high temperatures which is helpful for retaining manganese content. To improve the corrosion resistance, Chromium additions to Fe-Mn alloys have been widely studied. Chromium results in increased yield strength and flow stress resulting in enhanced wear property. Nitrogen is also a very strong austenite former and increases mechanical strength[9].

3.2 Alloy Development Process

Alloy powders with different compositions were iteratively deposited using the direct metal deposition technique (laser cladding technique). The powders were initially hand mixed and later in a rotating powder mixer at least for an hour to get uniform powder particle distribution. The powders were then sieved using sieving machine for 2 hours and the powder size between 45 microns 150 microns was used for deposition. The deposition took place 2 layers per cycle. After every 2 layers the deposition was rapidly cooled in nitrogen atmosphere for 3 minutes and the process was repeated again. The total process was repeated for 8 layers with total deposition thickness of 3mm approximately. All the samples deposited were of 1-inch square in size with 3mm thickness and the substrate used was stainless steel 316. After the samples were deposited, they were cut, mounted and polished using standard procedures.

3.3 Alloy-1: 22% Mn, 6% Al, 10%Cr, 0.1%C, 61.9 %Fe (in wt.%)

The alloy with above composition was deposited on stainless steel 316 substrate. After the deposition following analysis were carried out:
The results for Alloy-1 are shown below.

3.4.1 SEM ANALYSIS:

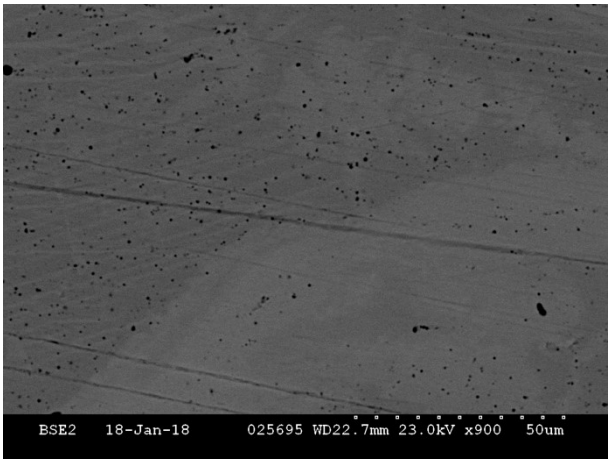

Figure 3.1 SEM of Alloy 1

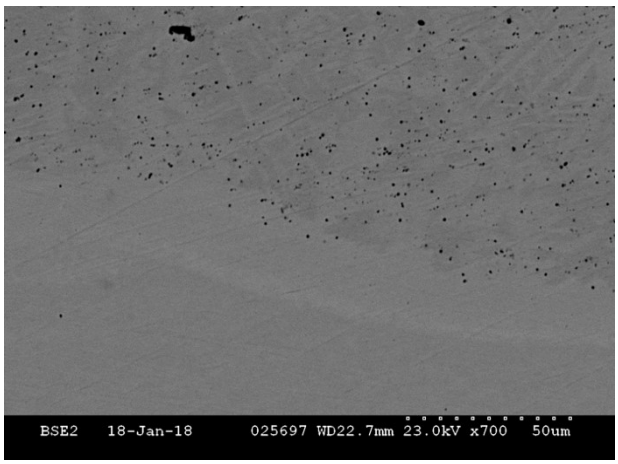

Figure 3.2 SEM of Alloy 1

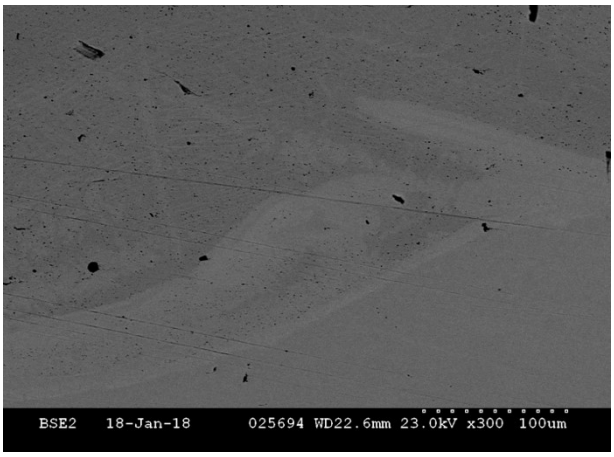

Figure 3.3 SEM of Alloy 1

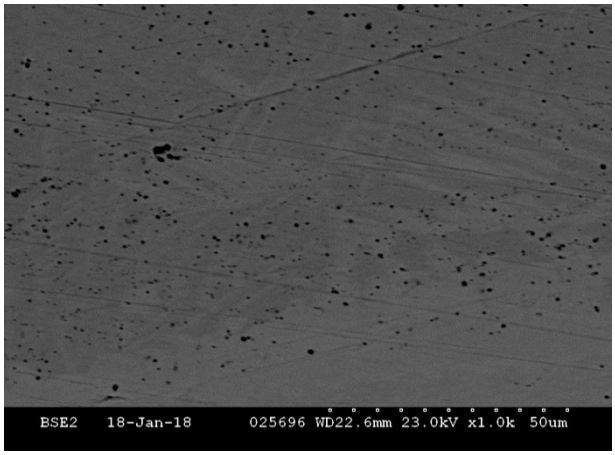

Figure 3.4 SEM of Alloy 1

The Figures (3.1-3.4) above show the cross-section of sample after polishing it to mirror finish. Both the images are of Alloy-1 observed under SEM. The figures show surface with 300X zoom, 700X zoom 900X zoom and 1000X zoom. Both images clearly show the interface of alloy with the substrate. The top half darker part is of Alloy-1 while the bottom half lighter part is of stainless steel substrate. The small black spots represent the pores in the samples.

3.4.2 EDS ANALYSIS:

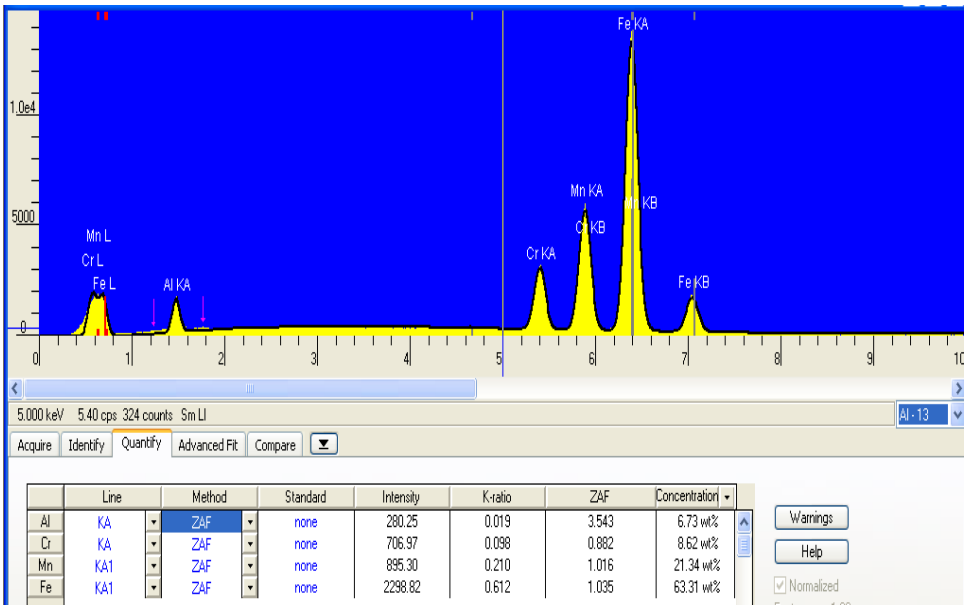

Figure 3.5 EDS of Alloy 1

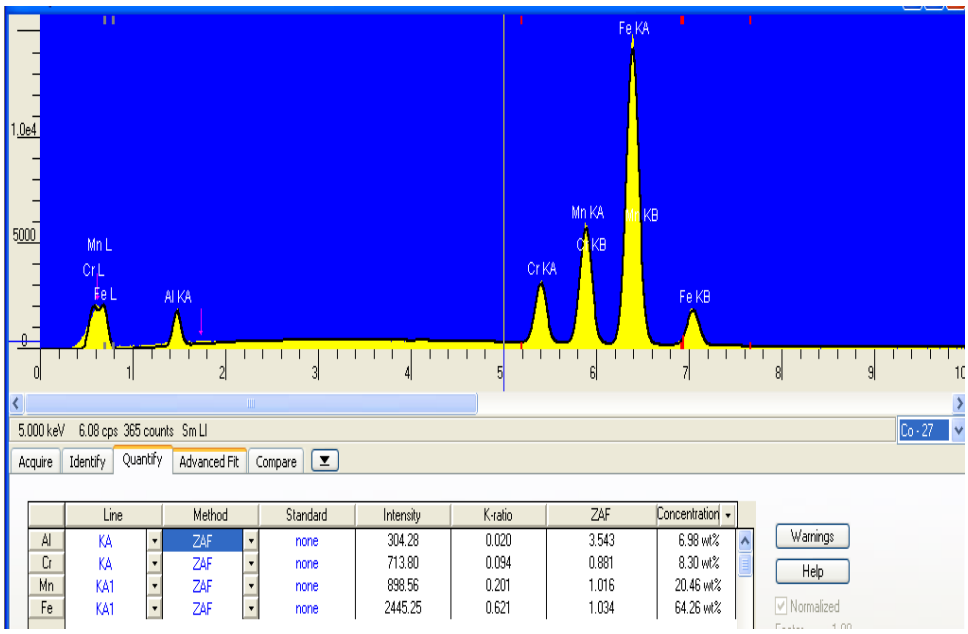

Figure 3.6 EDS of Alloy 1

Figure 3.5 and Figure 3.6 both show the composition of each element present in the sample. The distribution of aluminum is shown little higher compared to 6% as input. This could be because of aluminum is lighter compared to other elements. Both the EDS analysis were done at random place on deposition. There is 0.5-1.5% loss of manganese. This could be because of oxidation at

high laser power. The composition of carbon is not shown because of its 0.1% overall distribution which is very less compared to other element compositions to detect. Overall the composition is very similar to the input compositions.

3.4.3 HARDNESS:

Following figure shows the average hardness values for Alloy 1.

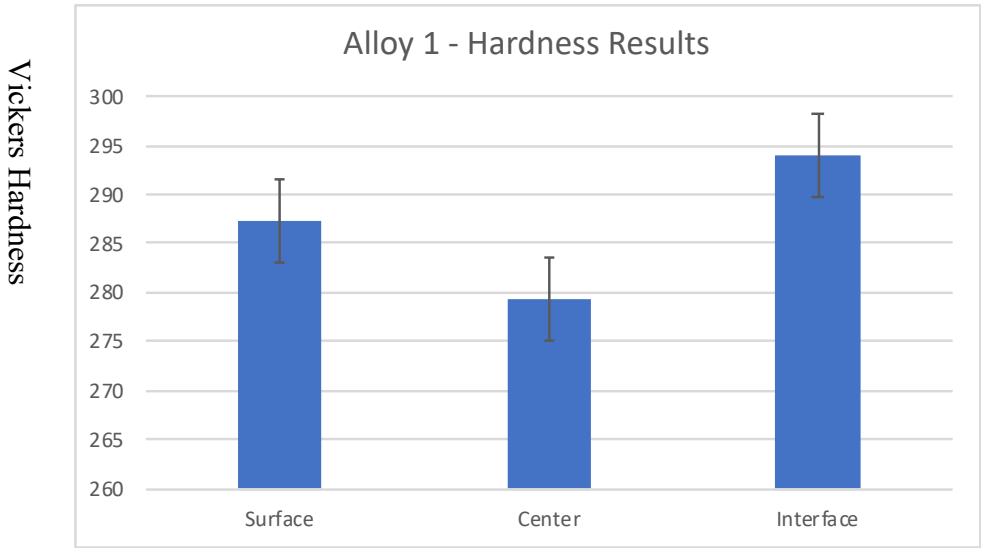

Figure 3.7 Hardness result for Alloy 1 on Vickers Hardness scale

The hardness values for Alloy-1 are between the range of 278-294. This shows a little variation in the distribution of elements. The hardness value at interface is little higher. This could be due to mixing of chromium from substrate while the initial layer was being deposited. The uniformity of hardness values throughout sample also confirms the uniform distribution of elements which was carried out by EDS analysis.

The hardness and wear properties can be further improved by performing nitriding process. Nitriding can be performed on either chromium, aluminum, iron, or manganese. Of all the elements of Alloy-1 manganese is the easiest to work on. Nitrides with chromium, aluminum, or iron are difficult to form and difficult to deposit because of the power required to melt chrome nitrides, aluminum nitride or iron nitrides is very high. However, manganese nitrides can be easily formed in pure nitrogen stream and is easy to deposit. For this study nitriding will be carried out on manganese to improve the properties of Alloy-1.

3.4.4 WEAR TEST & WEAR DEPTH:

The following Figure (3.8) shows the wear test results for Alloy 1 sample. The wear coefficient for Alloy 1 is around 0.4 $\pm$ 0.05.

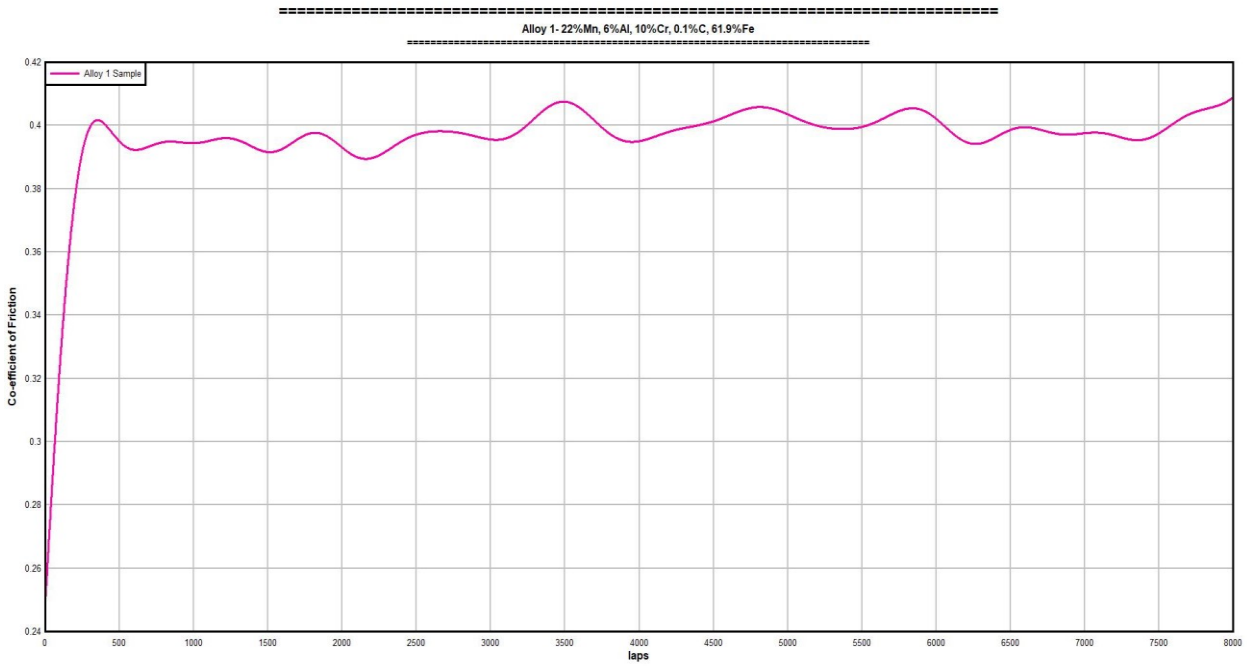

Figure 3.8 Wear result of Alloy 1

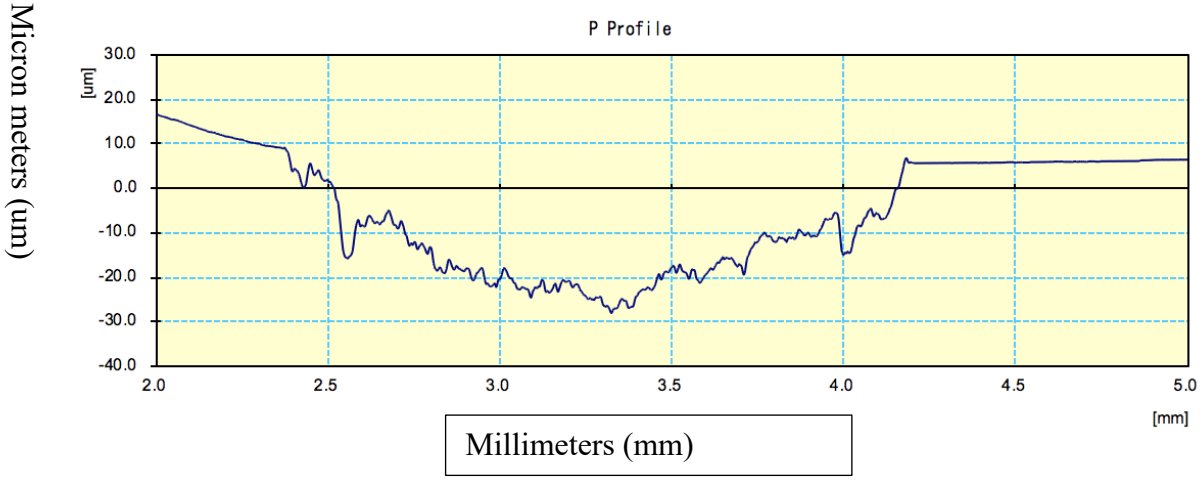

Figure 3.9 Wear Depth result of Alloy 1

The wear tests were repeated on the sample twice to confirm the uniformity of the results. Alloy-1 sample has shown good wear results compared to that of cast iron. The second figure shows the wear depth of the same sample. The width of wear profile was approximately 2mm and the depth was between -20µm to -30 µm.

3.4.5 CORROSION TEST

Following figure shows the corrosion result for Alloy 1. The x-axis shows the current density in logarithmic scale and the y-axis represents the potential in volts

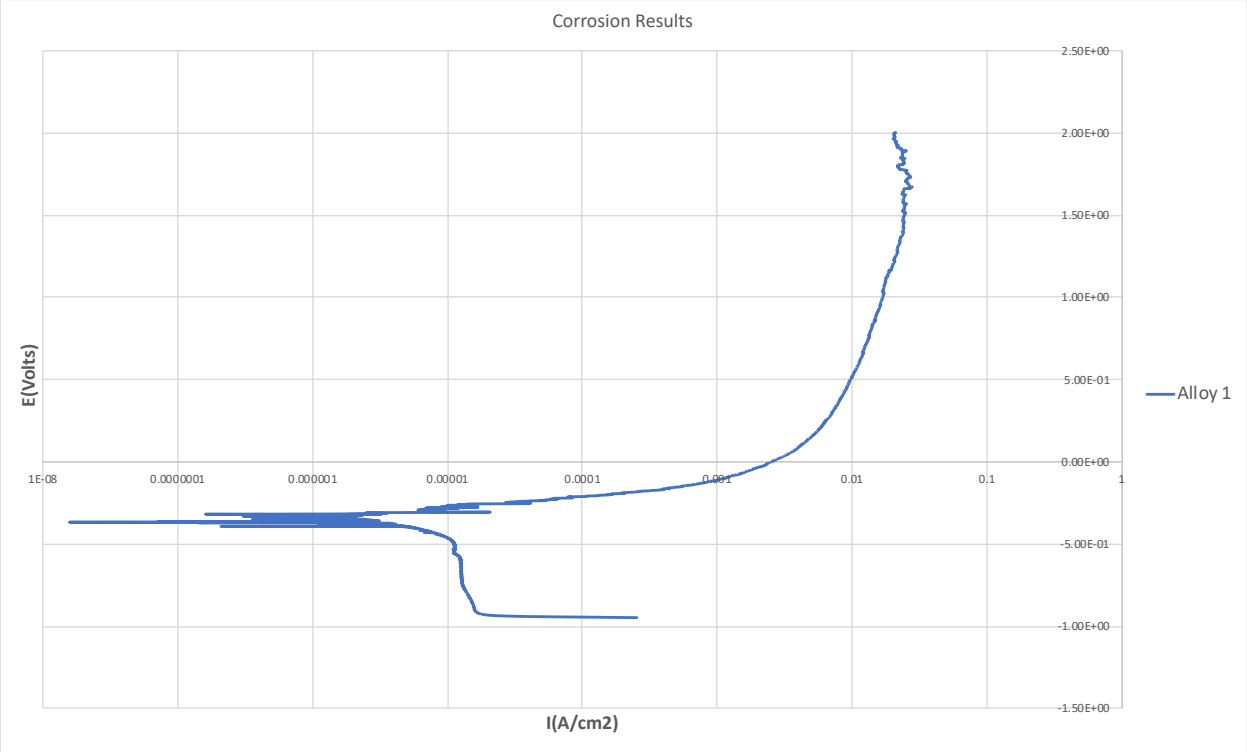

Figure 3.10 Corrosion results for Alloy 1 sample

Chapter 4 Nitriding

4.1 Nitriding Set-Up

Figure 4.1 Nitriding setup

The Nitriding experiments were carried out using following equipment:

1) Tube Furnace (Eurotherm Carbolite)
2) Mass Flow Controller (MKS Instruments)
3) Process Gas (90%H, 10%N) (100% N)

4) Quartz Tube

In this study a series of manganese nitrides were prepared by nitriding high purity (~99.9wt%) Mn Powders at various time and temperatures. Manganese nitride is usually produced by nitriding metallic Mn powder in nitrogen or in ammonia under ambient gas pressure. At elevated temperature manganese reacts with both nitrogen and ammonia. For this study the nitriding experiments will be carried out using Nitrogen (90%)-Hydrogen (10%) as a process gas. Literature data on the kinetics of formation of manganese nitrides and on the optimum conditions of synthesis of individual nitride phases are non-existent. Very few information is present about the properties of manganese nitrides. The manganese nitrides, Mn_4N is ferromagnetic and Mn_3N_2 is a paramagnetic. Manganese nitrides have unique magnetic properties. There are four stable phases ($\varepsilon, \eta, \zeta, \theta$) in the Mn-N binary system. The ζ phase ($Mn_6N_{2.58}$) has hexagonal closed-packed (hcp) structure. The ε phase (Mn_4N) has a face-centered cubic (FCC) structure. The η phase (Mn_3N_2) and θ phase (MnN) have face-centered tetragonal (FCT) structures[15]. For this study, 200 g of manganese powder was used for each experiment carried out. The powder size used was between 45μ to 150μ. The powder is nitrided in the corrugated glass tube which is rotated continuously throughout the whole process so that most of the powder is exposed to nitrogen flow. The process chamber was purged with nitrogen-hydrogen gas for 90 minutes to attain pure nitrogen filled atmosphere. After purge was completed the heating temperature and dwell time for that temperature was set using the furnace micro-controller. Mass flow meter was then used to control the flow rate of gas during the process. After the heating process was done the powder was cooled within the process chamber, while still under the protection of the nitrogen-based atmosphere, thus reducing the risk of distortion yet still improving the hardness, wear resistance and corrosion resistance properties. Phase analysis was carried out using the Rigaku Miniflex (Cu Kα radiation with $\lambda = 1.54020A$) XRD machine (Michigan Registration Num. 26423). The samples for X-Ray Diffraction analysis were prepared by coating the powder on black carbon tape and sticking the tape on a clear glass slide. The morphology and composition of the powder was studied using the scanning electron microscope (SEM) and energy-dispersive x-ray (EDX) detector. The powder samples for SEM and EDX analysis were prepared by coating powder on carbon tape mounted on an aluminum tub[10].

4.2 SEM Analysis

The morphology of nitrided Mn (Mn-N) Particles was analyzed using the SEM plan view secondary electrons (SE) imaging. The morphology of the nitrided powders is very similar for all experiments, hence images are presented for only one experiment. Irregular shaped particles with different sizes were observed. Fig 4.2 below shows SEM of Mn powder particles before nitriding and all other figures show after nitriding is done on the same powder. As it can be seen from the figures below nitrides are formed on Mn Particles as a result of process.

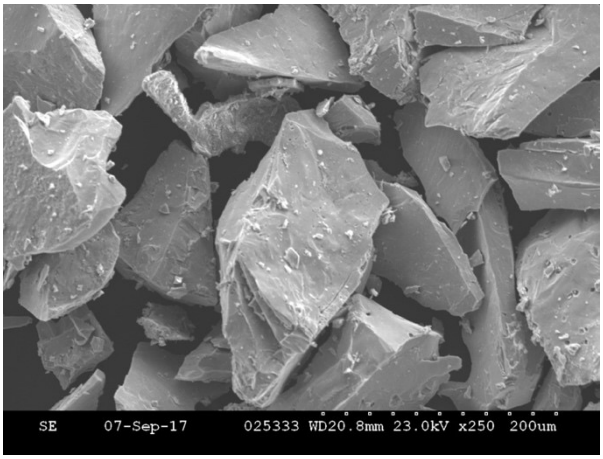

Figure 4.2 SEM of Manganese powder before Nitriding

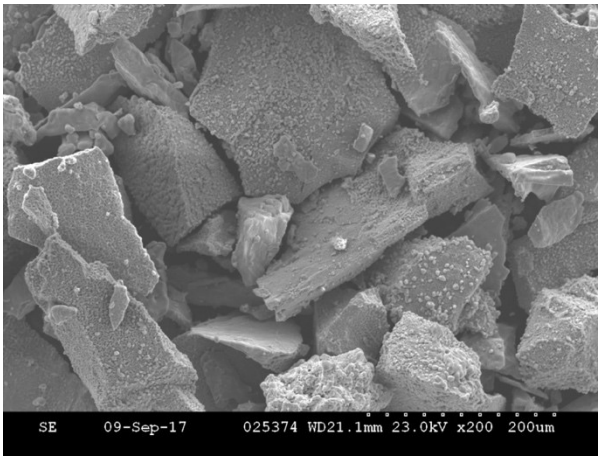

Figure 4.3 SEM of Nitrided powder

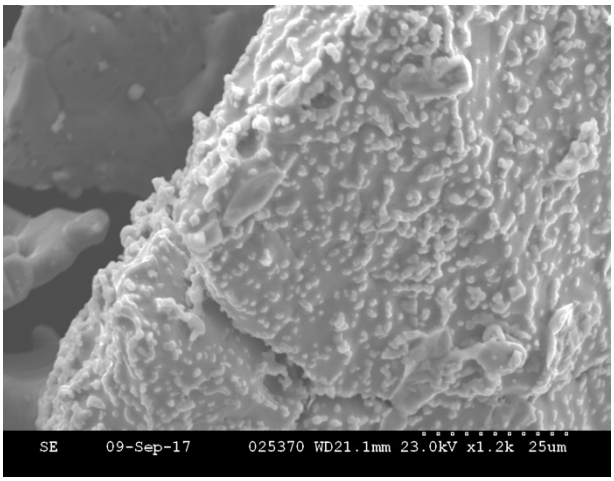

Figure 4.4 SEM of Nitrided powder

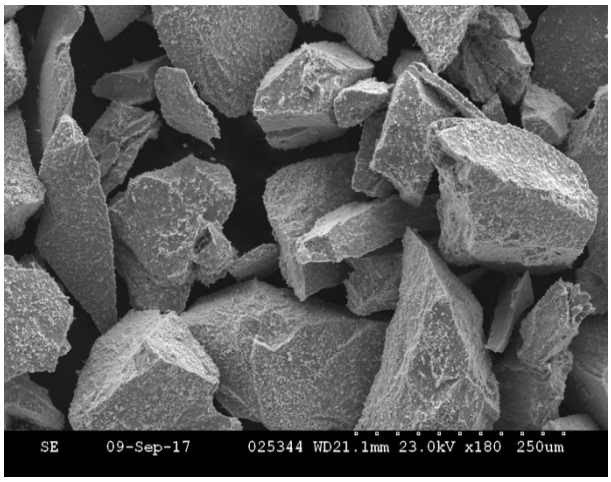

Figure 4.5 SEM of Nitrided powder

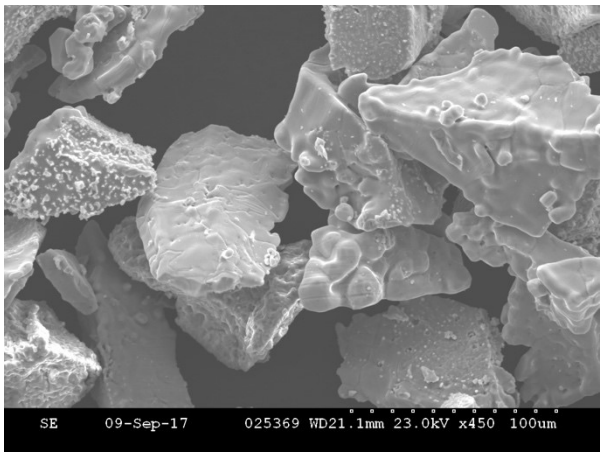

Figure 4.6 SEM of Nitrided powder

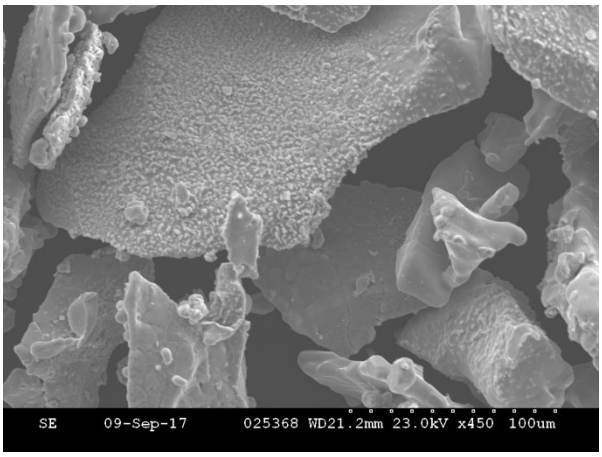

Figure 4.7 SEM of Nitrided powder

4.3 Cooling Rate

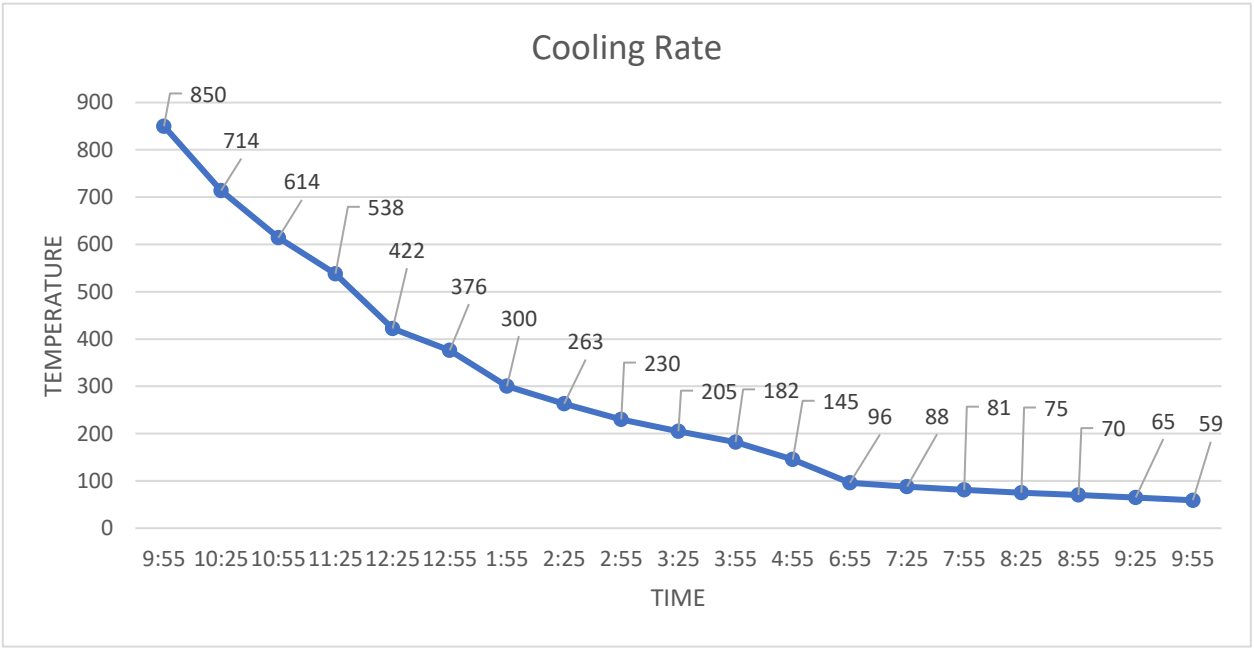

Figure 4.8 Cooling rate after Nitriding process

Above figure shows the kinetics involved in cooling of the Mn Powder after the nitriding process. Cooling is carried out in same process gas N_2H_2 stream in order to avoid contact with oxygen and reduce the chances of formation of oxides. As it can be seen from the plot it takes 12 hours approx. for temperature to drop to room temperature from 850°C. The initial temperature drop is quick and slows down as the temperature decreases.

4.4 Nitriding Parameters & Nitrogen Content

Table 3 Nitrided powders with parameters and Nitrogen Content

	Temperature (°C)	Time	Gas Flow Rate(SCCM)	Initial Purge Time(min)	Nitrogen Content (%wt.)
MnN(3)	850°C	4 Hrs.	30 SCCM	90 min	7.43%wt.
MnN(10)	1000°C	1 Hr.	30 SCCM	90 min	7.62%wt.
MnN(11)	575°C	12 Hrs.	30 SCCM	90 min	1.59%wt.
MnN(12)	850°C	4 Hrs.	15 SCCM	90 min	8.09%wt.
MnN(13)	1000°C	2 Hrs.	30 SCCM	90 min	8.08%wt.

4.5 Phase Analysis

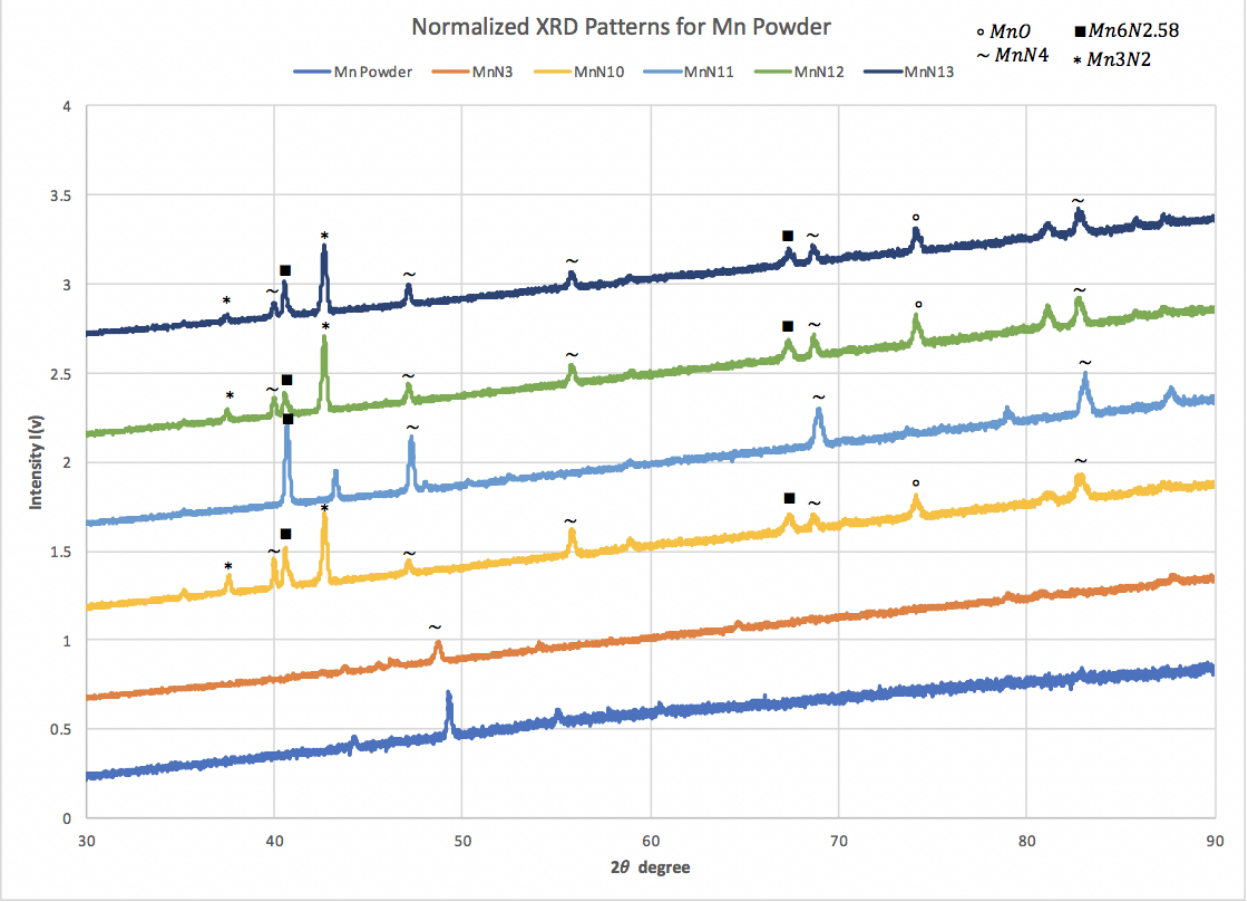

Figure 4.9 XRD patterns of Mn and nitrided Mn powder showing different phases

Fig (4.9) shows XRD pattern for Mn powder before nitriding along with patterns for nitrided powders at different time and temperatures. The nitrided powders are named as MnN(3), MnN(10), MnN(11), MnN(12), MnN(13) and the manganese powder without nitriding is named as Mn Powder. The parameters at which the powders were nitrided are provided in the table. The peaks from the XRD patterns for the nitrided powders can be ascribed to four separate phases i.e., Mn_4N, Mn_3N_2, MnO, $Mn_6N_{2.58}$. MnO phase is likely due to reaction with residual oxygen in the furnace. The amount of nitrides formed were investigated using LECO furnace method. It can be observed that the nitrides formed for MnN(11) powder is less (1.59%wt) compared to other powders. This is because of the low nitriding temperature of 575°C and longer time of 12 Hrs. Powders MnN(3) and MnN12 were nitrided using same time and temperature parameters but the gas flow for MnN(12) was reduced to half 15 SCCM that of MnN(3). This resulted in 0.66%wt more nitrogen absorption. A slight reaction between manganese and nitrogen can be observed at a temperature as low as 400°C. With rise in temperature the amount of nitrogen grows, attaining its maximum value at 800°C (nitriding time 25-60 min). As the temperature is still raised further, the nitrogen content of the reaction products slowly falls. At a temperature of 1100°C manganese nitrides are unstable and dissociates into the elements. As it can be seen from the patterns the formation Mn_4N phase is higher compared to other phases. The optimum condition for synthesis of phase Mn_4N are at temperature of 1000°C for 60 min[16].

Chapter 5 : Alloy Development with Nitrided Powders

For the second phase of alloy development nitrided powders were used. Manganese was nitrided in the lab, while commercially available aluminum nitride powder was used.

5.1 Alloy 2: 22% Mn(N13), 6% Al(N), 10% Cr, 0.1%C, 61.9%Fe (in wt.%)

The Alloy 2 was deposited with the same composition but instead of manganese and aluminum, manganese nitride and aluminum nitride powders were used. As discussed previously in the Nitriding chapter, nitrided powders are more stable and have good wear, corrosion and hardness properties. The deposition was once again carried out on stainless steel 316 substrate. Because of higher melting point of aluminum nitride and manganese nitride the deposition was done with 38 A for 8 layers.

5.2 SEM Analysis

From the SEM images it can be seen that the deposition with manganese nitride and aluminum nitride is better compared to Alloy 1. The sample has less pores and cracks.

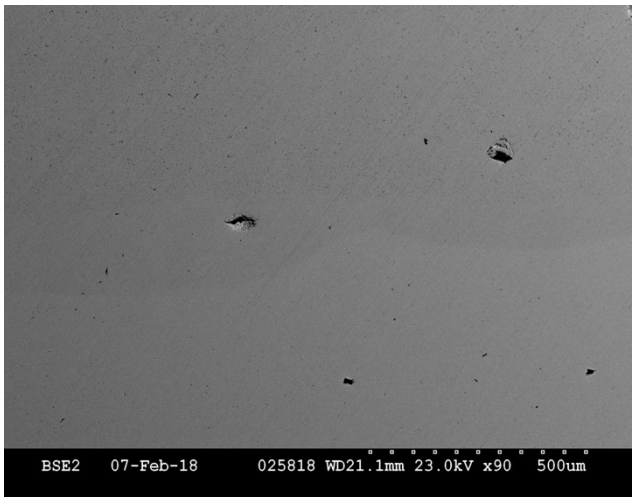

Figure 5.1 SEM of Alloy 2

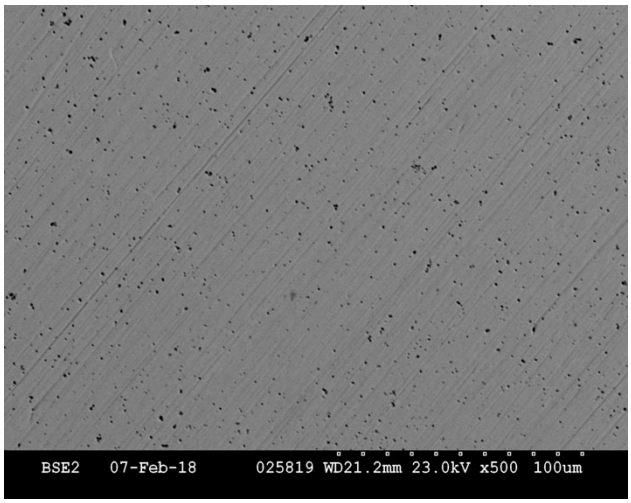

Figure 5.2 SEM of Alloy 2

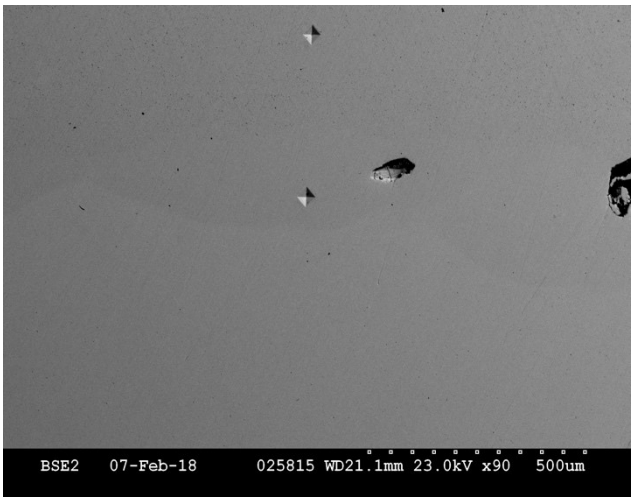

Figure 5.4 SEM of Alloy 2

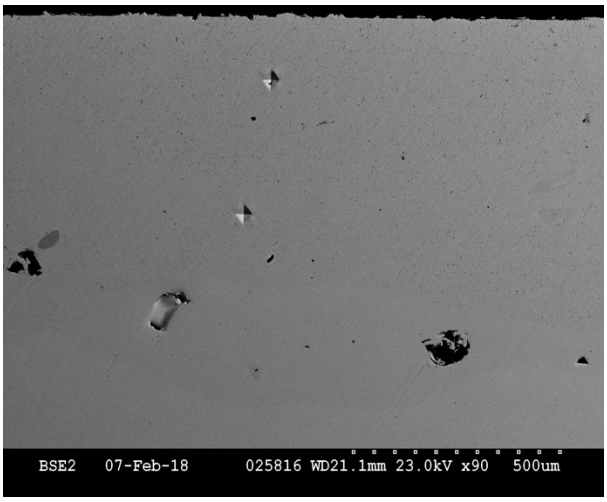

Figure 5.3 SEM of Alloy 2

5.3 EDS Analysis

The EDS analysis show us that some aluminum nitride is lost or hasn't been deposited. This is because of the high melting point of aluminum nitride compared to just aluminum. The other values are around the range of input values.

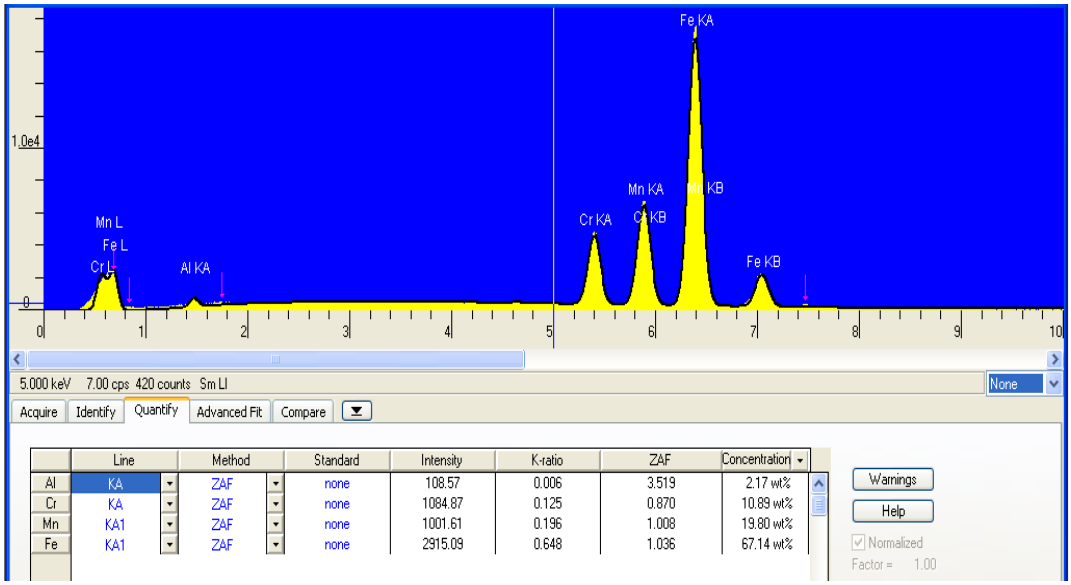

Figure 5.5 EDS of Alloy 2

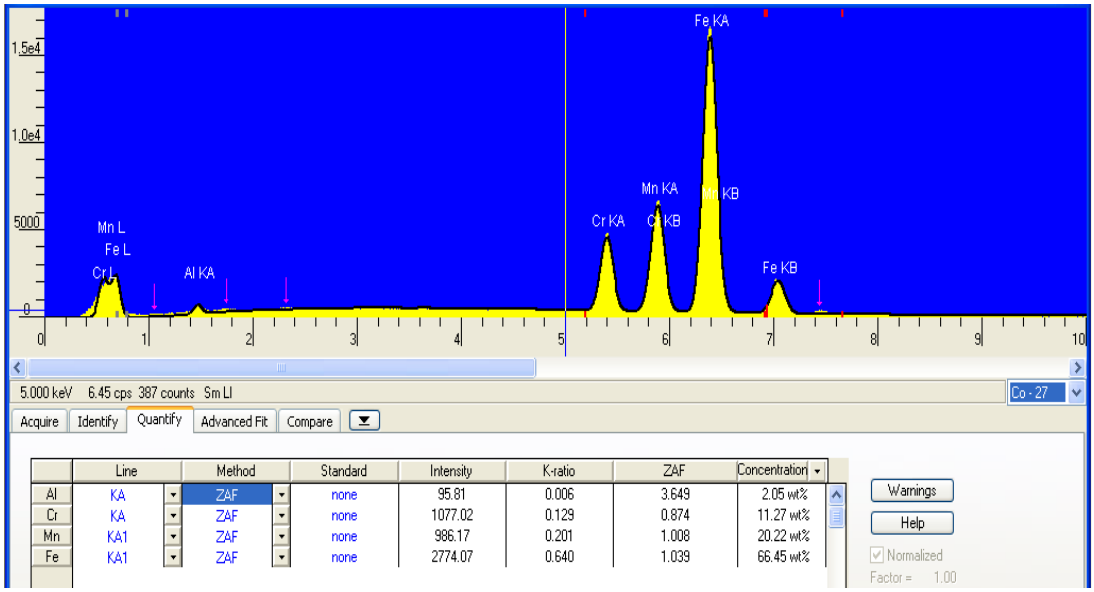

Figure 5.6 EDS of Alloy 2

5.4 Hardness

Following figure shows the average hardness values for Alloy 2 sample. The readings were taken in the similar points as the previous sample from Alloy 1. The hardness values for Alloy 2 are higher by 40 to 50 values compared to Alloy 1. This is a significant improvement in the hardness property for the alloy. The addition of nitrided powder has significantly improved the hardness property.

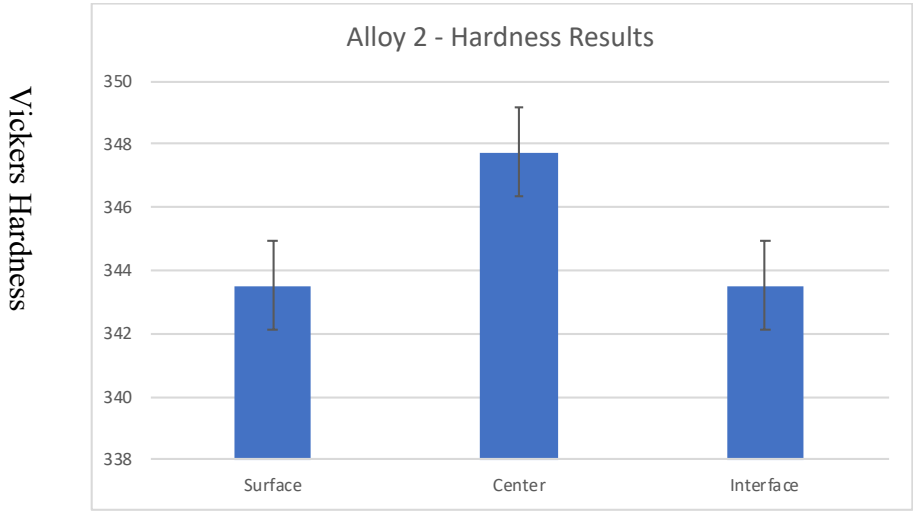

Figure 5.7 Hardness results of Alloy 2 sample on Vickers Hardness scale

5.5 Wear Test

The following figure shows the wear results for Alloy – 2 sample. The wear coefficient of friction coefficient for Alloy 2 is around 0.3±0.05. The wear coefficient of Alloy 2 sample is less compared to Alloy 1 which means the nitriding has improved the wear properties of the sample.

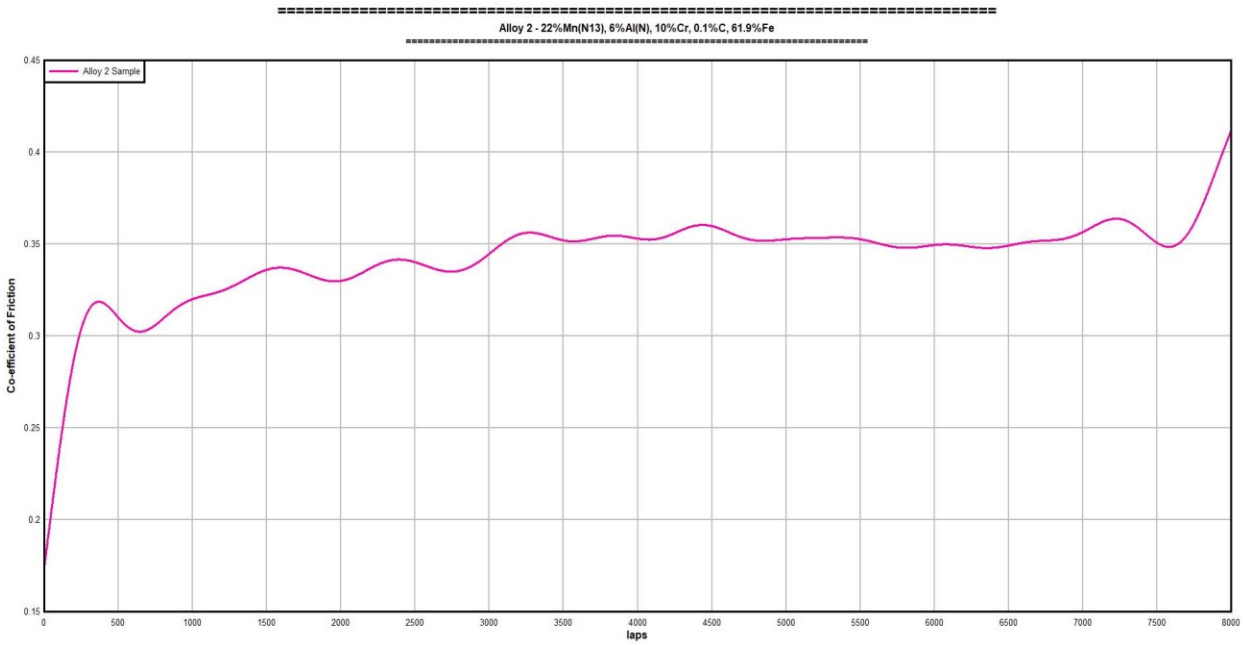

Figure 5.8 Wear result of Alloy 2 sample

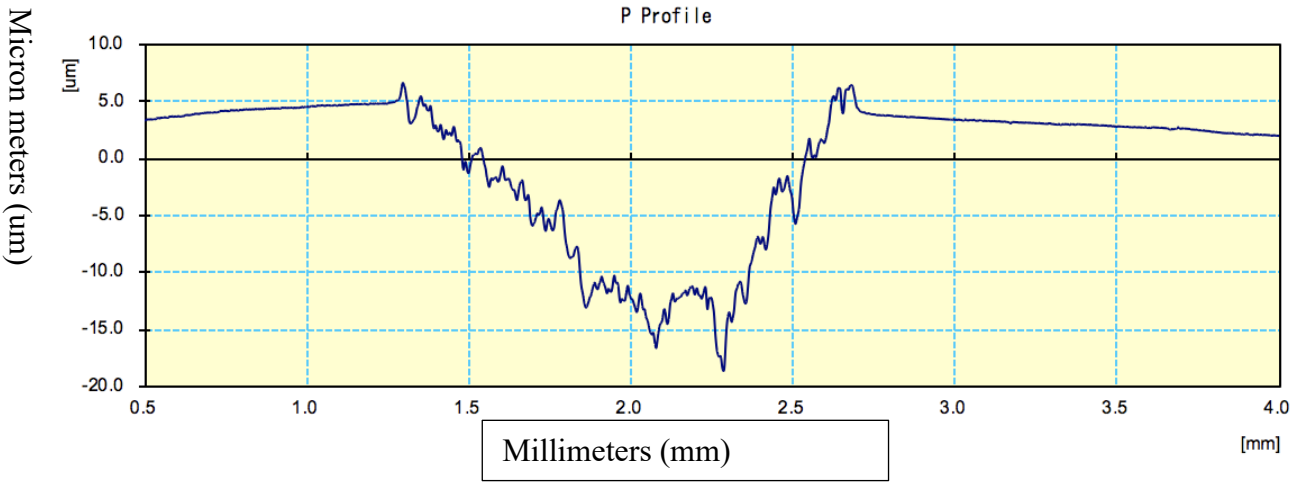

Figure 5.9 Wear result of Alloy 2 sample

Fig (5.9) shows the wear depth of the same sample. The width of wear profile was approximately 1.5 mm and the depth were between -10µm to -20 µm. The wear depth is less compared to Alloy 1 which means the Alloy 2 sample has worn less in comparison.

5.6 Corrosion Test

Following Figure (5.10) shows the corrosion result for Alloy 2. The x-axis shows the current density in logarithmic scale and the y-axis represents the potential in volts.

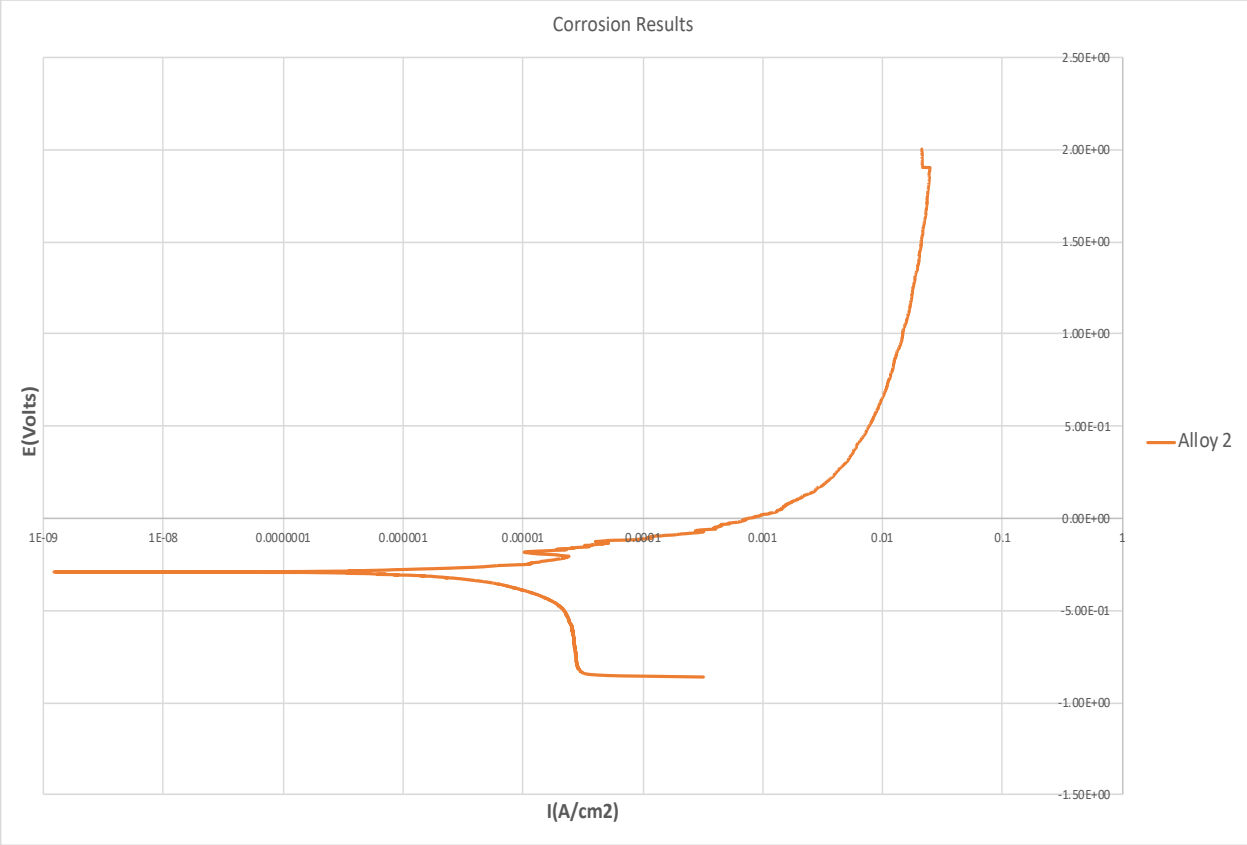

Figure 5.10 Corrosion result of Alloy 2 sample

Chapter 6 Results and Discussion

6.1 Wear Results

Following Figure (6.1) shows the wear results for Alloy 1 and Alloy 2 in in comparison with cast iron and stainless steel 316 samples. All the samples were tested for 8000 cycles for a load of 5 N. The total time for each wear test was around 2 hours 45 minutes. Each sample had been tested with new tungsten carbide ball. Both the alloys have better wear coefficient than cast iron and SS 316. For cast iron the wear coefficient varies greatly and is around 0.4 ± 0.2. For stainless steel 316 the wear coefficient is around 0.45 ± 0.05.

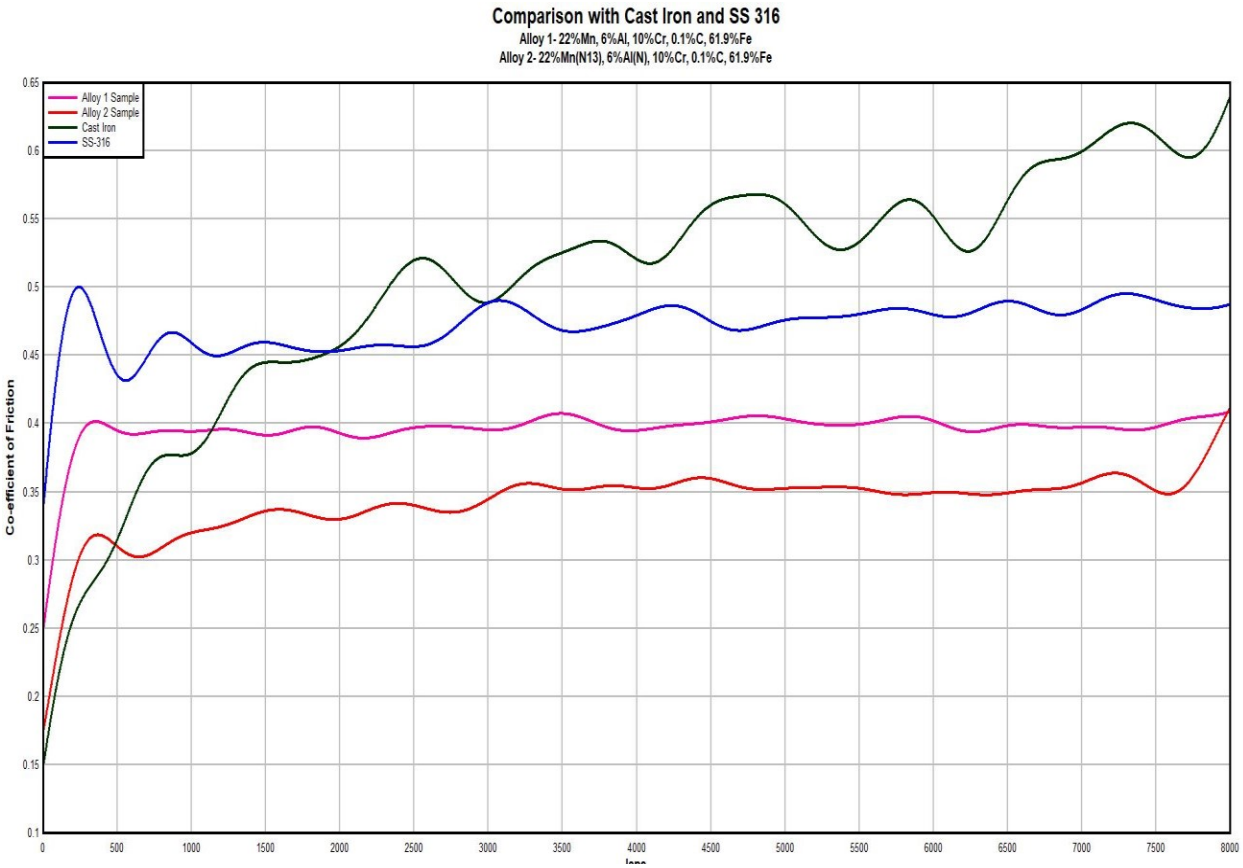

Figure 6.1 Wear comparison of Alloy 1, Alloy 2, Cast Iron, SS316

6.2 Hardness Results

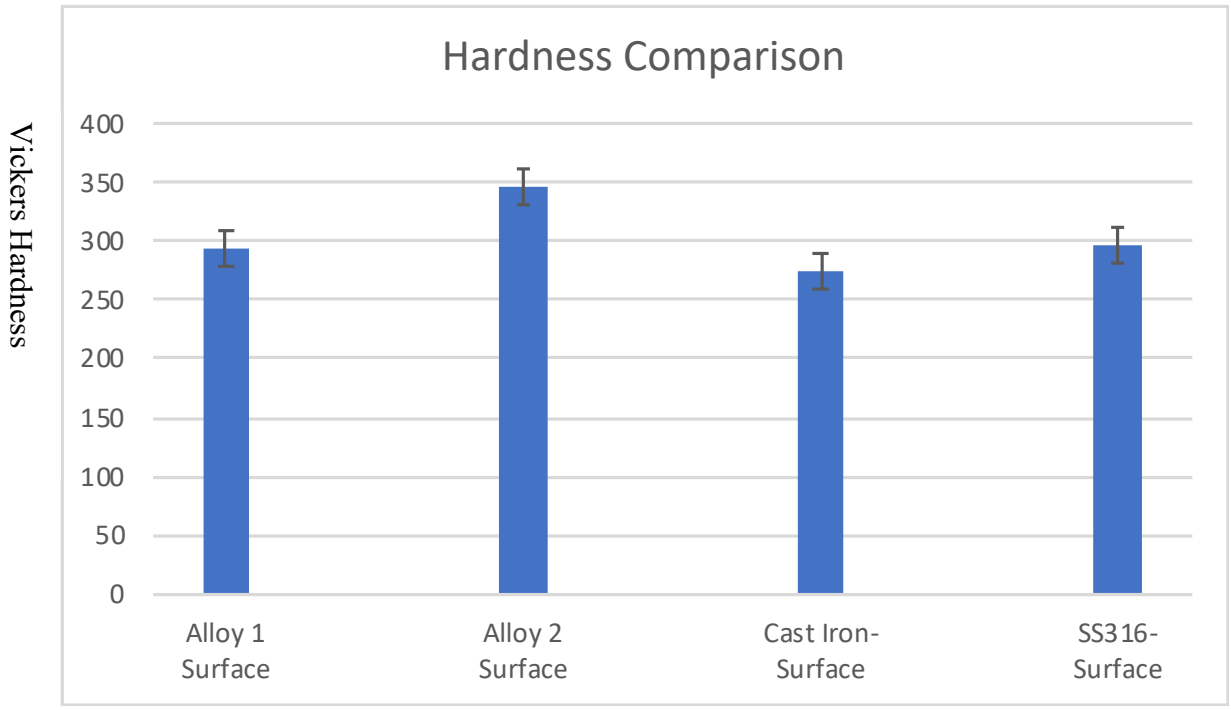

Figure 6.2 Hardness comparison of Alloy 1, Alloy 2, Cast Iron, SS-316 on Vickers Hardness scale

The above Figure (6.2) shows the hardness results for Alloy 1 and 2 in comparison with cast iron and stainless steel 316. The hardness readings are from the surface of samples. Total of 6 values were recorded at different places on the surface of sample and the average values were then plotted. The average value for Alloy 1 is 292.83 Vickers Hardness. For Alloy 2 it is 346.33. Vickers Hardness And for cast iron and SS 316 it is 275 Vickers Hardness and 295.5 Vickers Hardness respectively. Alloy 2 hardness is greater than both cast iron and SS316.

6.3 Corrosion Results

The corrosion tests on all the samples were carried out using AMETEK Princeton Applied Research (PAR) Flat Cell model K103. All samples were polished with grit emery papers starting with grade 240 up to 800 grade. The tests were carried in 0.5-wt. % NaCl solution prepared using analytical grade reagents. Following Figure (6.3) shows the results of corrosion test of Alloy 1 and Alloy 2 in comparison with cast iron and aluminum samples.

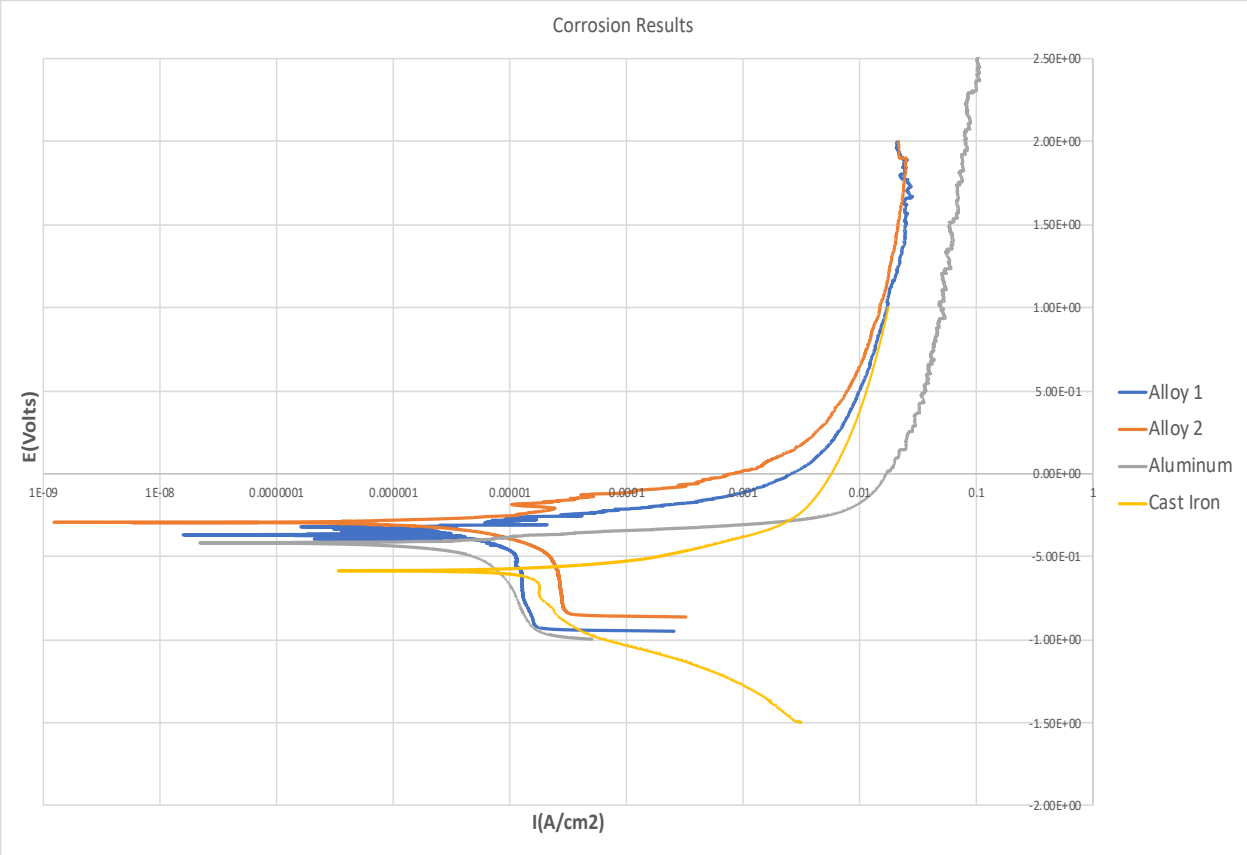

Figure 6.3 Corrosion result comparison of Alloy 1, Alloy 2, Aluminum, Cast Iron

Chapter 7 Conclusion

The goal of the study was to develop a low-cost wear and corrosion resistant coating material for aluminum alloys as an automotive brake rotor material. High manganese iron alloys present a potential solution and can be adapted to suit this application. Fe-Mn-Al-Cr-C alloys were laser clad onto stainless steel substrates with minimum dilution. A microstructure property evolution of these alloys was then performed to study the effects of alloying elements.

It is found that the Fe-Mn-Al-Cr-C alloy had better wear, corrosion and hardness properties compared to cast iron. To further improve properties a series of nitriding experiments were carried out at various time and temperature parameters using nitrogen-hydrogen as a process gas at ambient pressure. It is observed that multiple phases of manganese nitrides were formed during the process. It is shown that the only phase that can be purely synthesized using nitrogen as a process gas is Mn_4N. It was also established that nitride formation was higher with high temperature and less time as process parameters. According to X-Ray diffraction exposure of manganese to nitrogen for a period of 60 min to 240 min between temperature range of 575°C to 1000°C results in the formation of Mn_4N, Mn_3N_2, MnO, $Mn_6N_{2.58}$ phases with nitrogen absorption between 1.5%wt. - 8.08%wt.

Further Fe-Mn(N)-Al(N)-Cr-C alloy was tried with nitrided manganese and aluminum powders. The use of nitrided powder has improved the wear, corrosion, and hardness properties of the alloy.

Bibliography

[1] S. Mellor, L. Hao, and D. Zhang, "Additive manufacturing: A framework for implementation," *Int. J. Prod. Econ.*, vol. 149, pp. 194–201, 2014.

[2] E. C. Santos, M. Shiomi, K. Osakada, and T. Laoui, "Rapid manufacturing of metal components by laser forming," *Int. J. Mach. Tools Manuf.*, vol. 46, no. 12–13, pp. 1459–1468, 2006.

[3] J. W. Comb, W. R. Priedeman, and P. W. Turley, "FDM technology process improvements," *Solid Free. Fabr. Proc.*, pp. 42–49, 1994.

[4] J. J. Beaman, J. W. Barlow, D. L. Bourell, R. H. Crawford, H. L. Marcus, and K. P. McAlea, *Solid Freeform Fabrication: A New Direction in Manufacturing*. Boston, MA: Springer US, 1997.

[5] M. Feygin and B. Hsieh, "LAMINAlED OBJECf MANUFACTURING (LOM): A SIMPLER PROCESS."

[6] S. J. Michael Cima James Cornie Bredt A Curodeau M Estennan T Fan Kremmin S J Lee B Pruitt P Williams, "Three Dimensional Printing: Rapid Tooling and Prototypes Directly from CAD Representation."

[7] J. Mazumder, A. Schifferer, and J. Choi, "Direct materials deposition: designed macro and microstructure," *Mater. Res. Innov.*, vol. 3, no. 3, pp. 118–131, Oct. 1999.

[8] N. A. Waterman and P. Dickens, "Rapid Product Development in the USA, Europe and Japan," *World Cl. Des. to Manuf.*, vol. 1, no. 3, pp. 27–36, Jun. 1994.

[9] V. Varadaraajan, "Development of a novel iron-manganese alloy and its application," 2015.

[10] Z. Wang, "SiC Tile Encapsulation by Titanium / Titanium Alloy (Ti6Al4V): Manufacturing Process of Composite Plate Prototype for High Impact Applications Based on Additive Manufacturing Processes by," 2016.

[11] G. K. Lewis and E. Schlienger, "Practical considerations and capabilities for laser assisted direct metal deposition," *Mater. Des.*, vol. 21, no. 4, pp. 417–423, 2000.

[12] *DMD 105D Master Manual. Rep. N.p.: POM, 2008. Print.* .

[13] Wikipedia, "No Title." [Online]. Available: https://en.wikipedia.org/wiki/Scanning_electron_microscope.

[14] ThermoARL, "No Title." [Online]. Available: https://old.vscht.cz/clab/RTG/dokumenty/thermo/xrd/Introduction to powder diffraction.pdf.

[15] P. Z. Si *et al.*, "The high nitrogen pressure synthesis of manganese nitride," *Chinese Phys. Lett.*, vol. 29, no. 12, 2012.

[16] M. D. Lyutaya and A. B. Goncharuk, "Manganese nitrides," *Sov. Powder Metall. Met. Ceram.*, vol. 16, no. 3, pp. 208–212, 1977.